DEVELOPMENT OF CHEMOKINE-RELEASING MICROPARTICLES FOR THE MANIPULATION OF IMMUNE CELL RESPONSES

by

Allison Teunis
A Dissertation
Submitted to the
Graduate Faculty
of
George Mason University
in Partial Fulfillment of
The Requirements for the Degree
of
Doctor of Philosophy
Biosciences

Committee:

_____	Dr. Serguei Popov, Dissertation Director
_____	Dr. Lance Liotta, Committee Member
_____	Dr. Monique van Hoek, Committee Member
_____	Dr. Virginia Espina, Committee Member
_____	Dr. Iosif Vaisman, Acting Director, School of Systems Biology
_____	Dr. Donna Fox, Associate Dean, Office of Student Affairs & Special Programs, College of Science
_____	Dr. Peggy Agouris, Dean, College of Science
Date: _____	Spring Semester 2017 George Mason University Fairfax, VA

Development of Chemokine-Releasing Microparticles for the Manipulation of Immune Cell Responses

A Dissertation submitted in partial fulfillment of the requirements for the degree of Doctor of Philosophy at George Mason University

by

Allison Teunis
Bachelor of Science
James Madison University, 2011

Director: Serguei Popov, Professor
Department of Biosciences

Fall Semester 2017
George Mason University
Fairfax, VA

DEDICATION

This dissertation is dedicated to my amazing family (my parents Connie and Timothy, and my brother Ryan), including my wonderful fiancé Wally Hunt. Thank you for standing by me and keeping me sane. You have shared my feelings of success, as well as the many frustrations associated with research science. For these reasons and for all others which require no explanation, I dedicate this work to you.

ACKNOWLEDGEMENTS

I would like to express my sincerest gratitude to all the people who have directly helped with this research and who have indirectly helped by supporting me and shaping me into the curious, investigative person that I am today. This work would not have been possible without the guidance and expertise of my wonderful advisor, Dr. Serguei Popov. I owe much credit to Dr. Taissia Popova, especially for conducting many of the immunohistochemical staining procedures and sharing her evaluations. I have greatly valued my relationships with my committee members and researchers in other labs who have without hesitation been willing to teach me new techniques and have shared their equipment and/or reagents. Among them, Dr. Ruben Magni and Mrs. Kelsey Mitchell deserve special recognition for helping me through my many failed microparticle syntheses.

TABLE OF CONTENTS

LIST OF TABLES

LIST OF FIGURES

LIST OF EQUATIONS

LIST OF ABBREVIATIONS

Acrylic acid ..... AAc
Allylamine ..... AA
American Type Culture Collection ..... ATCC
Anthrolysin O ..... ALO
Bacillus anthracis (within figures) ..... B.a.
Bovine serum albumin ..... BSA
Chemokine ..... CK
Chemokine-loaded microparticle ..... CK-MP
Cibacron Blue F3GA ..... CB
Colony-forming unit ..... CFU
Complete serum-free medium ..... CSFM
Dendritic cell ..... DC
Dimethyl formamide ..... DMF
Dissociation equilibrium constant ..... K_d
Dithiothreitol ..... DTT
Edema toxin ..... ET
Enzyme-linked immunosorbent assay ..... ELISA
Extracellular-signal regulated kinases 1/2 ..... ERK1/2
Fetal bovine serum ..... FBS
Footpad ..... FP
Hematoxylin and eosin ..... H&E
High endothelial venule ..... HEV
Horseradish peroxidase ..... HRP
Interleukin-8 (CXCL8) IL-8
Keratinocyte-derived chemokine (Growth-regulated alpha protein; CXCL1) ..... KC
Kilodalton ..... kD
Kinetic dissociation constant ..... k_d
Lethal toxin ..... LT
Limulus amoebocyte lysate ..... LAL
Lipopolysaccharide ..... LPS
Lymph node ..... LN
Macrophage Inflammatory Protein 1α (CCL3) MIP-1α
Macrophage Inflammatory Protein 2 (CXCL2) MIP-2
Major Histocompatibility Complex II ..... MHCII
Microparticle ..... MP
Monocyte Chemoattractant Protein 1 (CCL2) MCP-1

N-isopropylacrylamide ..... NIPAm
N,N-methylene bisacrylamide ..... BIS
Penicillin and streptomycin..... Pen/strep
Phosphate-buffered saline ..... PBS
Polyacrylamide gel electrophoresis ..... PAGE
poly(lactide-co-glycolide acid) ..... PLGA
Post-infection ..... P.i.
Potassium persulfate ..... KPS
Protective antigen..... PA
Reactive Blue 4 ..... RB
Sodium dodecyl sulfate ..... SDS

ABSTRACT

DEVELOPMENT OF CHEMOKINE-RELEASING MICROPARTICLES FOR THE MANIPULATION OF IMMUNE CELL RESPONSES

Allison Teunis, Ph.D.

George Mason University, 2017

Dissertation Director: Dr. Serguei Popov

A confounding obstacle faced by the medical field is the ability of many disease agents to suppress the body's immune system which allows them to avoid elimination by the host. In this study, we have proposed a novel nanotechnology-based platform for achieving sustained delivery of immune-modulating chemokines (CKs) as a means for manipulating host immune responses. Functionalized hydrogel microparticles (MPs) were coupled with a variety of affinity baits and measured for their abilities to bind and release CKs. Favorable chemokine-loaded MP (CK-MP) pairs demonstrated affinities in the range of low micromolar to high nanomolar and maintained sustained CK release for more than 20 h *in vivo*. Upon injection in an established mouse model of subcutaneous hind footpad (FP) injection, a significant portion of the MPs accumulated in the regional draining lymph nodes (LNs). MP diffusion through the lymphatics and delivery by phagocytic cells to the LNs was advantageous as *Bacillus anthracis*, our model inducer of

immunosuppression, injected in this manner demonstrates the same distribution and localization in the host. Pre-treatment of spore-challenged animals with MPs loaded with neutrophil-attracting CKs (CK-MPs) provided significant protection against the infectious bacterium, even in the absence of any additional antibiotic intervention, although therapeutic (post-treatment) injection of the CK-MPs was not protective by itself. Both the bait-coupled MPs and their released CKs played important roles contributing to improved survival. The MPs induced endogenous expression of several pro-inflammatory cytokines and CKs to promote further stimulation of immune activity favorable for the host. Further mechanistic evidence for the protection conferred *in vivo* was that epidermal resident antigen-presenting cells (Langerhans cells) were activated and migrated to the local LN in response to CK-MP treatment. We propose further investigation into the potential clinical use of CK-MPs for achieving predictable, sustained modulation of immune activity.

INTRODUCTION

Innate immune response, key roles of chemokines

The innate immunity plays a prominent role in the clearance of infectious agents and tumors. In immune-sensitive conditions, the presence of microbial antigens sends danger signals which stimulate rapid responses from the innate immunity. This stimulation represents the coordinated activity of multiple cell populations and signaling pathways[1,2]. One key mechanism for the induction of an immune response is signaling *via* cytokines. Cytokines are small signaling proteins secreted by stimulated cells which elicit a response to damage or antigen detection from other cells. Among the cytokines, an important role belongs to chemokines (CKs), or chemotactic cytokines, for directing leukocyte migration. Binding of CKs with their specific G protein-coupled receptors expressed on distinct populations of leukocytes allows for induction of an appropriate response[3]. Stimulation of differing types of leukocytes can play distinct but often multiple and/or redundant roles. Examples of these roles may include phagocytic activity to clear a variety of undesirable antigen sources, angiogenesis to regulate blood vessel formation or wound healing in damaged tissues, and regulation of inflammatory responses[4,5]. The interaction between CKs and their target cell types occurs when CKs are released from stimulated host tissues into the surrounding tissue and lymphatics, where they form concentration gradients. Immune cells expressing the cognate

receptor(s) migrate up the CK concentration gradient toward the damaged or infected tissue, where the CK signal is highest[1,2].

Disease agents frequently evolve ways to circumvent or disrupt the immune response. One common mechanism involves induction of immunosuppression. Immunosuppression can occur through dysregulation of CK production by cells near the infected region, or by reducing the responsiveness of migrating immune cell populations through dysregulation of cellular signaling[6–8]. In both scenarios, disruption of normal CK-signaling pathways leads to conditions favorable for the pathogen. Current investigations are searching for effective methods for preventing microorganisms or tumor cells from evading the host immunity[9,10]. While therapies involving manipulation of leukocyte activity with CKs are promising, approaches based on their direct administration have been met with limited success in part due to the pharmacokinetic properties of CKs displaying functional instability and their rapid dissipation throughout the lymphatics upon injection[11–13].

Promising techniques designed to solve the problem of immune evasion involve the use of nanotechnology. Nanotechnology is an emerging area of research with utility in many different fields including medicine, manufacturing, bioremediation, energy, and electronics. In the field of medicine, nanoparticles and microparticles (MPs) (with diameter 1-100 nm and <1000 nm, respectively) have become important tools for the discovery of disease biomarkers[14], as vehicles for targeted-drug or other therapeutic molecule delivery[13,15–17], and for *in vivo*-imaging purposes[18].

MPs—what they are, how they are made. Current applications and favorable characteristics in support of our usage

One promising class of MPs consists of the non-toxic polyacrylamide hydrogel MPs. Many characteristics of these MPs can be manipulated during or after synthesis, making them a very versatile tool for specific research needs. Synthesis begins with radical-induced polymerization of N-isopropylacrylamide (NIPAm) crosslinked with N,N-methylene bisacrylamide (BIS)[14,19]. The concentration ratio of NIPAm and BIS used in MP synthesis can be manipulated to modify the average pore size of the MP products. The resulting insoluble gel precipitating out of solution has a three-dimensional thermoresponsive structure with porosity dependent on temperature. The MPs can be functionalized by co-polymerization with either acrylic acid or allylamine. This allows for the incorporation of a variety of chemical substances such as affinity dyes which can act as ligands (baits) inside the MPs.

The choice of organic dye baits can be tailored specifically for different biological applications and coupling chemistries[14]. Dyes that contain an amine group can be coupled to MPs functionalized with acrylic acid. A few of these dyes include Acid Blue 22, Remazol Brilliant Blue R, and Acid Black 1. Incorporation occurs *via* a condensation reaction in which the carboxylic group of the acrylic acid reacts with the amine group of the selected dye bait. For MPs functionalized with allylamine, reactive triazine dyes such as Reactive Blue 4 (RB) and Cibacron Blue F3GA (CB) can be incorporated into the MP by direct interaction with the amine group of allylamine. A chlorine atom located on a triazine ring of the dyes allows the dye to become substituted for the amine group of allylamine through a nucleophilic attack.

Once coupled with a dye bait, these MPs have multiple biological applications. One such application in the biomedical research field is for the discovery and identification of disease biomarkers[14,20]. Multiple studies have demonstrated that the hydrogel MPs with coupled dye baits can be added to biological samples, such as serum or urine, to concentrate and fractionate the low-abundance substances within their content for better sensitivity of detection[14,20]. Depending on the dye used, different types of proteins will become bound to the MPs through electrostatic, hydrophobic, or hydrogen-bonding interactions[21–23]. The lattice-like matrix of the MPs effectively excludes through size-sieving proteins larger than the particle size exclusion limit which could otherwise interfere with the assay, such as serum albumin. Elution using a small volume of an appropriate elution buffer can then allow for the concentration of proteins by over 100-fold to be within the range of detection of analytical techniques.

Another benefit of using MPs for collection and/or concentration of proteins is for stabilization and protection of bound proteins against degradation or aggregation[24]. This helps overcome the obstacle of rapid sample loss which can occur during the extraction procedure *in vivo* or upon handling *ex vivo*. The stabilized functional proteins or other biomolecules can then be released from the MPs upon elution or re-equilibration.

We have proposed that the hydrogel MPs with coupled affinity baits could be used as vehicles for the delivery of bound substances to different locations in the host followed by the release of these substances with controlled rate[25]. In this case, the MPs would function as a novel and potent nanotechnology-based research tool for multiple applications, including modulation of the host immune response. It is also likely that the

bait-functionalized MPs themselves (or in addition to the activity of the loaded cargo) may find utility as immune modulators due to their intrinsic adjuvant activity[26]. We anticipate that progress in this direction might result in the development of novel MP-based therapeutics applicable for a broad range of adverse immune conditions and infectious diseases which have characteristic dysregulation of host cell signaling.

Toward these goals, we focused on the modulation (remodeling) of the innate immune responses using MPs loaded with different CKs. We determined the behavior of the MPs *in vivo*, and analyzed the effects of MP-loaded CKs (CK-MPs) in animals challenged with a lethal infectious agent, *Bacillus anthracis* Sterne 34F2, as a model of an immunosuppressive disease known to impair immune cell migration[27].

Anthrax disease—infectious process, pathological features, current limitations to treatment, reasoning for selection as a model infectious agent

B. anthracis, a microbe that can be found in soil, is the causative agent of anthrax disease in both humans and animals. More worrisome than this pathogen's natural occurrence is its potential for use as a biological weapon. Infection with anthrax spores can occur *via* inhalational, gastrointestinal, and cutaneous exposure. The first stage of infection irrespective of the infection route is typically asymptomatic and involves rapid phagocytosis of the spores by macrophages and dendritic cells (DCs), resulting in their delivery from an infected tissue to the regional lymph nodes (LNs). Germination of the spores and proliferation of the vegetative bacteria at this site result in the severe hemorrhagic lymphadenitis and edema observed in patients during the second symptomatic stage[28,29]. Current therapies against anthrax are limited in efficacy against

late-stage infection, as inhalational anthrax has an 80% mortality rate when left untreated[30] and a 45% mortality rate even after the administration of antibiotic therapy[31]. This is in part due to the fact that antibiotics poorly penetrate the LNs, as dormant spores have been found in these sites after antibiotic therapy completely removed the vegetative bacilli from the bloodstream[32]. Therefore, a successful immune response during early stages of infection in the LNs is predicted to be a critical point at which therapeutic intervention could promote host survival. We hypothesized that modulation of the host immune response by CK-MPs could be protective in animals challenged with *B. anthracis* spores.

This bacterium possesses a multitude of virulence factors which contribute to its pathogenicity. Some of the major virulence factors recognized in this species are the edema toxin (ET) and the lethal toxin (LT). ET and LT are composed of a cell-binding pore-forming component, protective antigen (PA), associated with the edema and lethal factors, respectively. Toxins' production by germinating spores within the LNs disrupts the functions of immune cells such as dendritic cells (DCs), including their ability to release inflammatory CKs for the recruitment monocytes and neutrophils[27,33–36]. Of the disrupted cell populations, the significance of neutrophil migration during anthrax infection is unclear. Several reports describe conflicting evidence on the necessity of targeting neutrophils for the establishment of infection[37–40]. Another major virulence factor is the poly-γ-D-glutamic acid capsule which further protects the proliferating bacteria against phagocytosis and shields against detection, allowing the bacteria to survive the host's immune surveillance.

This species also contains several other virulence factors, including four hemolysins. One of these which is also a pore-forming toxin with cytolytic activity, anthrolysin O (ALO), has recently been discovered as an important contributor to *B. anthracis* toxicity[41]. ALO belongs to a family of cholesterol-dependent cytolysins, with highly homologous proteins encoded by several other species including *Bacillus cereus*, *Listeria monocytogenes*, *Clostridium perfringens*, and *Streptococcus pyogenes*. Although the precise mechanism by which it contributes to virulence is unclear, ALO has been implicated in playing a key role at the stage in which vegetative bacilli escape from the phagolysosome[42]. Current models suggest that the concerted action of ALO and three phospholipases expressed in the early anaerobic conditions within macrophages allows the bacteria to escape into the cytosol. It is additionally suggested that anaerobic fermentation products, including succinic acid produced during anaerobic bacterial growth, function synergistically with ALO to induce membrane permeabilization and cause release of free radicals from the mitochondrion, ultimately resulting in cell death[43].

Current study

Overall, the combined activities of these virulence factors to allow escape from the initial innate immune response and to evade other responding immune cells spark interest for how *B. anthracis* infection might be impacted by immunomodulation favorable to the host. We demonstrate here that novel CK-MPs can be used to remodel the host immune response and that timely stimulation of beneficial immune cell populations by the CK-MPs can improve survival in anthrax spore-challenged mice.

RESEARCH AIMS

Microorganisms frequently evolve the ability to avoid or overcome a host's immune response, thereby causing pathogenesis. We hypothesized that a novel nanotechnology-based platform based on the controlled release of immune-modulating substances by bait-coupled hydrogel MPs could remodel the host immune response to promote the body's ability to clear an infection.

This hypothesis was tested in the experimental system consisting of the bait-coupled hydrogel MPs loaded with different immune cell-attracting CKs for their controlled-rate release within regional LNs after subcutaneous challenge in mice. The effect of MPs on the immune status of LNs and their potency to eliminate the infectious agent (*B. anthracis*) was investigated.

This dissertation research was conducted to investigate the following specific aims:

Aim I. Characterize *in vitro* hydrogel MPs as a tool for controlled loading and sustained release of selected CKs

(a) Demonstrate the abilities of MPs to bind and release CKs. (b) Examine the influences of the physical characteristics of the system (including buffer composition and temperature) on the capabilities of MPs to bind and release CKs. (c) Evaluate the specific affinities and kinetics for multiple CK-MP pairs.

Aim II. Characterize the behavior and activity of MPs injected subcutaneously in a mouse model

(a) Determine the impact of MP-released CKs on directing immune cell trafficking to regional LNs in mice subcutaneously challenged with the MPs using immunohistochemical staining for the target cell populations. (b) Analyze the significance of CK-MPs *vs*. potential intrinsic adjuvant properties of MPs and *vs*. soluble injected CKs for sustained immune modulation to the regional LN.

Aim III. Evaluate the protective effectiveness of CK-MPs in animals challenged with an immunosuppressive agent

(a) Demonstrate the effect of CK-MPs on the bactericidal activity of immune cells in regional LNs and survival of *B. anthracis*-challenged mice as a proof-of-principal prophylactic treatment approach against infectious disease. (b) Identify major variables contributing to the mechanism(s) of immune remodeling and associated protection seen in anthrax spore-challenged mice.

RESEARCH DESIGN

Materials

N-Isopropylacrylamide (NIPAm), N-N′-methylenebisacrylamide (BIS), potassium persulfate (KPS) and allylamine (AA), were purchased from Sigma-Aldrich, Cibacron Blue F3GA was purchased from Polysciences, Inc. Unless specified otherwise, all other reagents were from Sigma-Aldrich, and were used as received. Water for all reactions, solution preparation, and polymer washing was distilled/purified using a Millipore Milli-Q water purification system to a resistance of 18 MΩ and passed through a 0.2 μm nylon filter. Recombinant mouse CCL3 (MIP-1α), CCL2 (MCP-1), CXCL2 (MIP-2), and human CXCL8 (IL-8) were carrier-free from BioLegend. Cell culture media and reagents were purchased from Mediatech, Inc. The CyQUANT NF Cell Proliferation Assay Kit was from ThermoFisher Scientific. Endotoxin-free water was from Life Technologies. *B. anthracis* Sterne strain 34F2 was from Colorado Serum Co. α-*B. anthracis* serum recognizing the vegetative bacterium was raised in rabbits after a subcutaneous spore challenge.

Synthesis of MPs

MP synthesis was carried out essentially as described by Longo *et al*[24]. pNIPAm particles with ~7% molar content of acrylic acid (AAc) relative to the total monomer were prepared *via* precipitation polymerization. NIPAm (9.0 g) and BIS (0.28 g) were

dissolved in 250 mL of water, and the solution was then partially degassed by vacuum filtration through a 0.45 μm nylon filter. The filtered solution was purged with nitrogen at room temperature and a medium rate of stirring for 15 min, before AAc (0.5 g) was added to the reaction. Following the addition of AAc, the solution was purged with nitrogen for another 15 min and then heated to 75°C. Once the reaction mixture had attained a stable temperature of 75°C, polymerization was initiated with the addition of KPS (0.1 g) in 1.0 ml of water. The reaction was maintained at a constant temperature of 75°C with stirring under nitrogen for 3 h. After this time, the reaction was allowed to cool to room temperature overnight with stirring under nitrogen. For preparation of NIPAm functionalized with allylamine, the AAc was replaced with allylamine (676 μl, 12 μmoles). The particles were then harvested and washed by centrifugation for 20 min at 23°C and 16,000 g, with the supernatant subsequently discarded. The pelleted particles were then re-suspended in 300 ml of water, and the suspended particles pelleted by centrifugation. This centrifugation-dispersion process was repeated for a total of 5 times. Particles were stored as a suspension in water with a few drops of chloroform as an antimicrobial.

Cibacron Blue F3GA (CB) and Reactive Blue 4 (RB), reactive triazine dyes, were immobilized *via* direct reaction with the amine group of the allylamine units within the particles, displacing the lone chlorine on the disubstituted triazine ring of the dye[22]. Reactive Blue MPs were a kind gift from Ceres Nanoscience, Inc. Trypan Blue was coupled to the MPs by condensation of the amino group of the dye to the carboxylic group of acrylic acid present in the pNIPAm-co-AAc MPs using activation with N-(3-

dimethylaminopropyl)-N′-ethyl carbodiimide as described by Castro-Sesquen *et al*[44]. After the incorporation of the dyes, the particles were harvested and washed in water by 5 cycles of centrifugation-dispersion for 20 min at 23°C and 16,000 g, with the supernatants discarded. Finally, MPs were re-suspended in water with a few drops of chloroform as before. To demonstrate the absence of bacterial contamination, 100 µl of particle suspension were plated on the Luria broth agar and incubated for up to 48 h at 37°C. The N4 Plus PCS Submicron Particle Analyzer (Beckman Coulter) was used to determine the particle size (400-700 nm) and polydispersity index in water, which was in the interval of 0.2 to 0.5.

Additional CB MPs were prepared under sterile, endotoxin-free conditions. The MPs were re-suspended in tissue culture-grade endotoxin-free water and incubated with the dye (2 g CB dye per 325 ml of total solution) for 24 h or 48 h at room temperature. After dye incorporation, the MPs were washed six times using tissue culture-grade PBS diluted 1:3 with endotoxin-free water. The absence of bacterial contaminants was demonstrated as described above by plating onto Luria Broth agar plates. Similarly, a few drops of chloroform as a bactericidal agent were added to the final batch of MPs stored at 4°C.

Determination of MP endotoxin contamination

The endotoxin content of MPs was measured with the Pierce Limulus Amoebocyte Lysate (LAL) Chromogenic Quantitation Kit (ThermoFisher) according to the manufacturer's protocols. The *E. coli* endotoxin standard provided in the kit was serially diluted with the endotoxin-free water. The supernatant from MP suspensions

prepared under the endotoxin-free was collected for analysis. Supernatant and diluted standards were incubated with the kit's synthetic substrates at 37°C for 6 min, and the endotoxin-dependent proteolysis of the substrate was measured at 405 nm as the amount of released p-nitroaniline after quenching of reaction with acetic acid. MPs prepared using the endotoxin-free conditions contained 0.14 EU/ml of endotoxin.

Analysis of CK binding using ELISA and Western blot

The sandwich ELISA Ready-SET-Go! IL-8 and MCP-1 kits (eBioscience) were used according to the manufacturer's protocols to measure the IL-8 and MCP-1 binding to the Cibacron and Reactive Blue MPs. The CKs supplied with the kits were diluted with PBS to concentrations of 0.25 to 1.0 ng/ml and mixed with equal volumes of MPs washed 3x with PBS by pelleting the MPs at 16,000 g for 5 to 10 min and re-suspending the pellet in a fresh portion of PBS. Different dilutions of the stock suspension (5% wet pellet *v/v*) were used. The mixtures of MPs with CKs were incubated for indicated periods of time at 4°C, the MPs were pelleted at 16,000 g for 5-10 min at room temperature, and the supernatants were withdrawn for analyses. Triplicate wells in 96-well plates were used for supernatants and control dilutions of the standard CKs.

For western blot analysis, the samples of the supernatants and pelleted MPs were mixed with standard 2x SDS-PAGE loading buffer (Invitrogen) supplemented with DTT, boiled for 5 min and loaded on 4-20% polyacrylamide gel. Protein bands from the gel were transferred onto a nitrocellulose membrane using iBlot Gel Transfer Device (Invitrogen) and probed with the CK-specific polyclonal antibodies (from Biolegend for MIP-2 and LifeTechnologies for IL-8) followed by the appropriate secondary antibodies

conjugated with horseradish peroxidase. SuperSignal West Femto Maximum Sensitivity Substrate (Pierce) was used to generate chemo-luminescence of the protein bands, which was measured with a Molecular Imager ChemiDoc XRS System (Bio-Rad). The relative intensities of bands were calculated after densitometry using the QuantityOne 4.6.5 software (Bio-Rad). As determined using control measurements with different amounts of CKs tested in triplicates within the same experiment, the standard deviations (SD) of relative band intensities were in the range of 7 to 17% (n=3).

Labeling of pNIPAm-co-AA MPs with Alexa Fluor 555

Alexa Fluor 555 (Invitrogen) is a bright orange dye widely used in fluorescent imaging. It is water-soluble and pH-insensitive from pH 4 to 10. The succinimidyl ester of Alexa Fluor 555 was used for conjugating the dye to primary amines on pNIPAm-co-AA MPs. For this purpose, 100 µl of MPs were washed 2x with 1 ml of 50 mM bicarbonate buffer, pH 8.3, re-suspended in 500 µl of the buffer, and mixed with 50 µl of the dye solution (1 mg in 100 µl of DMF). After 1 h at room temperature, the particles were washed 3x with 1 ml of PBS (pH 7.4) and finally re-suspended in 500 µl of PBS. The particles were observed at 555/570 nm using Olympus BX51 microscope with a TRITC filter set. The number of labeled MPs was counted after appropriate dilution and was found to be about 7×10^5 per 1 µl of original suspension. The particles suspended in water had an average size of 520±54 nm with a dispersion index of 1.0±0.3 indicating a slight tendency to aggregate.

Overall, the fluorescent particles were well dispersed and migrated readily through the lymphatics when injected as described in the “Administration of MPs into

Animals" section below. For injection into the hind leg footpads (FPs) of mice, the MP suspension was mixed with equal volume of 2% tracer dye Evans Blue in PBS. This dye allowed us to locate the LNs during surgery and did not quench the fluorescence of Alexa Fluor 555. The LNs were collected and prepared as described below and the particles were observed as described here.

Loading of MPs with CKs

Loading of the MPs with CKs for *in vitro* assays was accomplished by incubating CB MPs (10% wet *v/v*) with 1 μg/ml of indicated CK in 1/3 PBS at 4°C overnight. The buffer was supplemented with 100 U/ml of penicillin and 100 μg/ml streptomycin (pen/strep) to prevent bacterial contamination. The MPs were pelleted, supernatants removed, and the MP pellets were re-suspended in the culture medium for chemotactic assays as described below. Suspensions of CK-MPs used for animal injections were prepared by incubating CB MPs (10% wet *v/v*) in PBS with a mixture of IL-8 and MIP-1α (1 μg/ml each) at 4°C overnight. The suspensions were brought up to room temperature and injected into FPs of mice as described for animal challenge experiments below.

In vitro chemotactic assays for immune cell migration analysis

In vitro chemotactic assays were conducted in a 96-well format. The transwell inserts incorporating tissue culture-treated polycarbonate membrane filters (8.0 μm pores) from Neuro Probe, Inc. were used. Cell migration of monocytic human THP-1 cells from ATCC was measured. The bottom chambers of the transwell plates contained 300 μl of

complete serum-free medium (CSFM) from Mediatech with or without MIP-1α or IL-8. The CK solutions were assayed at several concentrations up to 100 ng/ml. The CB MP-bound CKs were assayed after their release from the MPs. For this purpose, the MPs loaded with MIP-1α or IL-8 were incubated in CSFM at 37°C for 3 h. The MPs were removed by centrifugation and the supernatants containing released CK were transferred into bottom wells of the transwell plate. Dilutions of supernatants were prepared in the transwell plate immediately prior to assay performance. To increase the chemotactic responsiveness of migrating cells, the cells were starved in CSFM at 37°C, 5% CO_2 for 1 h prior to assay. The serum-starved cells (50 μl of $1.28x10^7$ cells/ml) were added to the top chambers. Cell migration after 4 h at 37°C, 5% CO_2 was enumerated by the DNA-binding fluorescent dye using the CyQUANT NF Cell Proliferation Assay Kit (Thermo Fisher Scientific) according to the manufacturer's protocols. Briefly, cells from the bottom chambers were pelleted by centrifugation, incubation medium was removed, and the cells were permeabilized using the kit's dye delivery reagent to allow the dye to associate with nuclear DNA. After 10-min incubation at room temperature in the dark, the stable fluorescence of DNA-dye association was measured using a fluorimeter at 485/538 nm. Fluorescence intensity was converted to the fraction of migrated cells using calibration curves obtained from known numbers of cells.

The number of cells trapped on the membrane that were unable to fully migrate to the bottom chamber was estimated after staining with Crystal Violet. For staining, the membranes were rinsed 3x with PBS and fixed with methanol for 15 min, incubated with 3% Crystal Violet stain (Becton Dickinson) at room temperature for 15 min, washed 3x

with water, and air-dried. The cells were counted under a microscope. Less than 0.1% of the total cell number were retained on the membranes, and were therefore not considered for calculations.

Viability analysis of Raw 264.7 cells exposed to MPs

To test the effect of MPs on Raw 264.7 cell viability, the cells were grown to 60-70% confluency in a 96-well plate in DMEM/F12 containing 10% FBS. Cells were starved for 1 h in 100 µl/well of serum-free DMEM/F12. Medium was then removed and replaced with 100 µl samples. Samples included control serum-free medium, CB MPs diluted to give 10%, 3.3%, or 1.1% of pellet volume, and the hydrolyzed CB dye diluted to give 10-fold, 3.3-fold, or 1.1-fold molar excess over its concentration in the MPs. The MPs were pre-washed three 3x in PBS, 1x in serum-free DMEM/F12, and re-suspended in fresh serum-free DMEM/F12. To account for a possible effect of LPS contamination, LPS from *E. coli* L3012 serotype O111:B4 was used at 10 µg/ml. After cell exposure for 24 h the samples were removed, cells were washed 3x with 100 µl of warm PBS, and 200 µl of Alamar Blue in CSFM (Corning) were added. Fluorescence was measured after 2 h with excitation at 530 nm and emission at 590 nm.

Administration of MPs into animals

All animal procedures were performed under the approval of George Mason University's Institutional Animal Care and Use Committee. Female 6- to 8-week-old DBA/2 mice (Jackson Labs) received food and water *ad libitum* and were subcutaneously challenged in both hind FPs with 50 µl Reactive Blue MP suspensions or control CK

solutions, 3 animals per challenge group. The MPs (5% wet *v/v*) suspension contained either 0.1 ng/µl or 1 ng/µl of each IL-8 and MIP-1α. Control solutions contained the same amounts of CKs without MPs, or the MPs without CKs. The mixtures were incubated overnight at 4°C and then used for animal inoculations. Groups of mice were euthanized at 30 min, 4 h, and 24 h post inoculation. Thirty min before euthanasia, the animals were anesthetized *via* isoflurane inhalation and 20 µl of 1% tracer dye Evans Blue in PBS were injected into the hind FPs. In some experiments the dye solution contained fluorescent nanoparticles. The LNs were surgically removed into 10% neutral buffered formalin solution for histological evaluation. After fixing in formalin, the tissues were embedded in paraffin, the paraffin blocks were sliced into 8 µm sections, and mounted onto glass slides for standard hematoxylin/eosin (H&E) staining and further microscopic evaluation.

A separate experiment was conducted in which animals (n= 2-3) were administered AA MPs with/without the coupled CB dye with/without loaded CKs (1 µg/ml each of MIP-1α and IL-8). MPs suspensions (10% wet *v/v*) delivered as a 50 µl volume in PBS were subcutaneously into both hind FPs of mice. Animals were injected with Evans Blue in PBS 30 min prior to euthanasia after 24 h. LNs and FPs were removed for immunohistochemical staining.

Administration of MPs into animals with *B. anthracis* spore challenge

Groups of female 6- to 8-week-old DBA/2 mice were challenged with *B. anthracis* Sterne 34F2 spores in PBS into each hind FP. At certain times before and/or after the spore challenge, mice received 50 µl subcutaneous FP injections of MPs (10% wet *v/v*) with or without loaded CKs, as well as the CKs only, by the same route as

spores. The number of mice per group (from 5 to 10) and the spore doses (from $1.6x10^4$ to $4x10^6$ spores delivered in 20 or 50 µl of PBS into each hind FP) are indicated in the corresponding figure legends. The animals were monitored once or twice daily and were euthanized by carbon dioxide asphyxiation if one or more of the following criteria were met: (1) Rough hair coat, hunched posture, distended abdomen, or lethargy if debilitating, (2) Respiratory distress (dyspnea) or cyanosis, (3) Central nervous system signs such as head tilt, tremors, spasticity, seizures, circling, or paresis, (4) Persistent lateral recumbency, (5) Impaired mobility interfering with eating, drinking, or ambulation. Analgesics were not administered due their potential interference with the infectious and inflammatory processes. All injections were performed under anesthesia using isoflurane inhalation for chemical restraint and reduction of stress.

Thirty minutes before euthanasia, the animals were injected with 20 µl of 1% Evans Blue dye in PBS into both hind FPs for visualization of LNs. One popliteal LN and both hind FPs from each animal were placed in 10% neutral buffered formalin solution for immunohistological analysis. The formalin-incubated tissues were embedded in paraffin blocks, sliced into 5 µm sections, and mounted onto glass slides for staining. For enumeration of bacterial titers, the other popliteal LN from each infected animal was homogenized using frosted glass slides and suspended in PBS. Volumes of 10 µl and 100 µl of homogenized tissue suspensions were plated onto Luria Broth agar plates and incubated at 37°C overnight.

Semi-quantitative scores of FP inflammation and edema were assigned immediately prior to Evans Blue dye injection as: 0= no visible signs, 1= initial signs of

swelling and light redness in the FP, 2= prominent swelling and redness partially extending from the FP to the ankle, 3= strong swelling and redness extending to the whole ankle, 4= extensive swelling and redness beyond the ankle. The statistical significance of inflammation scores was determined using a two-tailed Mann-Whitney U test. Mortality curves were compared using the Log Rank Test.

Immunohistochemical analysis

Slides used in immune cell staining were subjected to antigen retrieval in sodium citrate buffer (pH 6) for 40 min at 95°C followed by incubation for 20 min at room temperature. For slides stained with the anti-bacterial serum, the incubations at 95°C and room temperature were 20 min each. All slides were stained with antibodies using a Dako autostainer and counter-stained with Mayer's hematoxylin.

For staining using the non-biotinylated antibodies (α-myeloperoxidase to detect neutrophils, CD11b for monocytes/macrophages, TNF-α, MHCII, and pERK1/2) or immune serum against *B. anthracis*, sections after antigen retrieval were incubated in 3% hydrogen peroxide in methanol for 5 min to inhibit peroxidase activity, blocked with Dako Protein block for 5 min, and then incubated with a primary antibody (myeloperoxidase Ab9535 from Abcam, dilution 1:50; CD11b Ab133357 from Abcam, dilution 1:4000; TNF-α Ab9739 from Abcam, dilution 1:200; MHCII antibody PA5-22113 from Invitrogen, dilution 1:200; pERK1/2 antibody 9101 from Cell Signaling, dilution 1:200; α-*B. anthracis* serum, dilution 1:100) for 30 min, followed by anti-rabbit EnVision+ HRP-Labeled Polymer (Dako). Colorimetric detection was completed with diaminobenzidine for 5 min, and slides were counterstained with Mayer's hematoxylin.

As an exception, colorimetric detection of MHCII and pERK1/2 in consecutive tissue slices involved the use of diaminobenzidine (brown) or Emerald green (green), respectively, where notated.

To detect the presence of Ly-6G$^+$ neutrophils in other experiments (as notated), tissue sections after antigen retrieval were incubated with the primary biotin-labeled Ly-6G antibody (Biolegend; rat anti-mouse clone 1A8, dilution 1:200) followed by the Dako CSA streptavidin-biotin-peroxidase complex. Antibody staining was completed with a 5-minute incubation with 3,3'-diaminobenzidine tetrahydrochloride and followed with counter-staining using Mayer's hematoxylin.

Effect of the MPs on *B. anthracis* spores and vegetative bacteria

The MPs and the CB dye contained in the particles were tested for their effect on the *B. anthracis* spore germination and vegetative bacterial growth. MPs or CB dye were incubated in a 2-ml total volume with *B. anthracis* Sterne 34F2 spores per well in a 12-well plate. Wells without spores were included as controls for each sample. The final concentrations in the appropriate wells were: 800 spores/ml, 5% pellet volume of MPs, or the CB dye diluted to concentration corresponding to its expected content in the MPs after coupling (concentration of allylamine used during MP synthesis; 40 μM). The reactive chlorine of the dye was hydrolyzed during its incubation in a carbonate buffer to account for its removal in the coupling reaction. MPs or dye were incubated with spores for 24 h or for 0 h (spores added to medium immediately before collecting samples) at 37°C. After incubation, 1 ml of each sample was collected and pelleted at 8,600 g for 10 min. Supernatants were removed and replaced with 1 ml of Alamar Blue in CSFM.

Samples were incubated at 37°C with Alamar Blue for 1 h, centrifuged again, and 200 µl from each sup was plated 3x in a 96-well plate. Fluorescence of the dye was read at 530/590 nm using a plate fluorimeter.

MP stimulation of endogenous immune mediators by Raw 264.7 cells

Raw 264.7 cells were grown as 2-ml cultures per well in 12-well plates until 80-90% confluency using DMEM/F12 medium supplemented with 10% fetal bovine serum (FBS). Cells were serum starved in 1 ml serum-free DMEM/F12 for 1 h and then exposed to 1 ml of samples which included the MPs (at 10% pellet volume with or without a coupled CB dye with free allylamine amino groups), control serum-free DMEM/F12, 10 µg/ml LPS from *E. coli* L3129 serotype O127:B8, and the hydrolyzed CB dye diluted to concentrations corresponding to 10-fold, 3.3-fold, and 1.1-fold molar excess over its content in MPs. At the indicated times, sups were collected and centrifuged to pellet the MPs. All supernatant samples were supplemented with 0.5% BSA for protein stabilization, frozen at -20°C, and then analyzed using ELISA or the Bio-Plex Pro™ Mouse Cytokine 23-plex Assay (Bio-Rad) according to the manufacturer's protocol. The Bio-Plex kit's standards were reconstituted and diluted in serum-free DMEM/F12 containing 0.5% BSA. Samples and standards were loaded onto the kit's magnetic beads for 30 min, washed, and incubated with the secondary detection antibody for 30 min, followed by streptavidin-peroxidase conjugate for 10 min. After washing and final re-suspension in the kit's assay buffer, the magnetic beads were analyzed using the Bio-Plex machine at low photomultiplier settings (RP1).

To be within the detection range for ELISA, sups for detection of MCP-1 after 4-h and 24-h cell exposure to the MPs were diluted from 5- and 10-fold, respectively, with a serum-free DMEM/F12 with 0.5% BSA. MP- and dye-treated samples for detection of TNF-α were diluted 10- and 50-fold, respectively. Only the treated 24-h supernatants were analyzed for MIP-1α and KC. The treated supernatants for MIP-1α analysis were diluted 5-fold and undiluted for KC analysis. The supernatants of controls (cells only) were undiluted for detection of TNF-α, MCP-1, and KC, whereas those for MIP-1α analysis were diluted 5-fold.

AIM I

MPs containing different chemical baits can be loaded with CKs

We investigated hydrogel MPs composed of NIPAm and crosslinked with BIS, which were functionalized with either acrylic acid (AAc) or allylamine (AA). Multiple batches of MPs were characterized by their light scattering properties and the average particle diameter in PBS at 25°C was between 400-700 nm with a standard deviation of 3 to 17 nm, and with pore sizes sufficient to allow diffusion of proteins smaller than 20 kD. The polydispersity index was low (between 0.2 and 0.4), indicating a low level of aggregation.

Different baits can be coupled to functionalized MPs to generate MPs potentially capable of maintaining a sustained release of CKs with a range of different affinities. An important molecular property for the interaction of CKs with bait molecules is the relatively small size (8-10 kD) of CKs to allow for unimpeded diffusion into and within the MP gel. The CK polypeptide chains also possess a high positive charge favorable for electrostatic interaction with the anionic baits at physiological pH. Therefore, to capture CKs by MPs we chose baits capable of electrostatic and hydrophobic interactions through sulfonic groups and substituted aromatic rings in their structures.

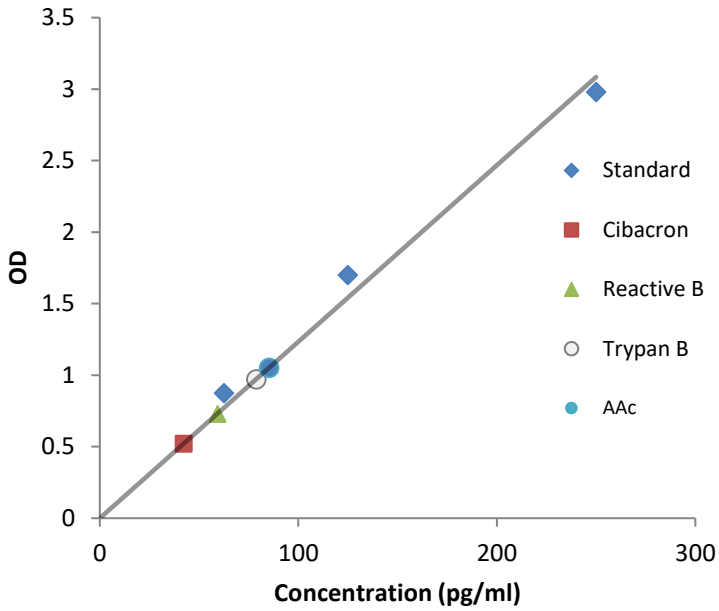

Figure 1. ELISA of IL-8 binding achieved by MPs containing a variety of chemical baits.
The concentration of IL-8 (from 250 pg/ml) unbound in solution after incubation with MPs (5% wet *v/v*) for 30 min at room temperature is shown. Concentrations of IL-8 in the supernatant after incubation with CB, RB, Trypan Blue, or AAc uncoupled MPs were calculated according to the standard curve represented by blue diamonds.

MPs containing different types of anionic dye baits were tested for their ability to capture the neutrophil-attracting CK, IL-8 (Figure 1). The baits included AAc without an associated dye, AAc coupled with Trypan Blue, and AA coupled with Reactive Blue 4 (RB) or Cibacron Blue F3GA (CB). PBS at pH 7.4 was used as a buffer to mimic the physiological characteristics of blood and lymph. The amount of CK binding was determined by analyzing the concentration of remaining unbound CK in supernatant after a brief 30-min incubation of IL-8 with the MP suspensions. CB was the best for binding IL-8 as it successfully removed 84% of IL-8 from solution, followed by RB, Trypan Blue, and AAc which respectively bound 76%, 68%, and 66% of the CK.

Decreased ionic strength of buffer increases binding of CKs to MPs

To demonstrate the contribution of electrostatic interactions, MPs coupled with the RB bait were incubated with the neutrophil-attracting chemokine MIP-2 (200 ng/ml) in PBS and in PBS diluted 1:3 at 4°C overnight. In the latter case, almost no detectable unbound CK was found in the supernatant when analyzed using Western blotting, whereas in the undiluted PBS a faint band remained (Figure 2). The MPs were also eluted by boiling with SDS-PAGE loading buffer and the eluted material was examined.

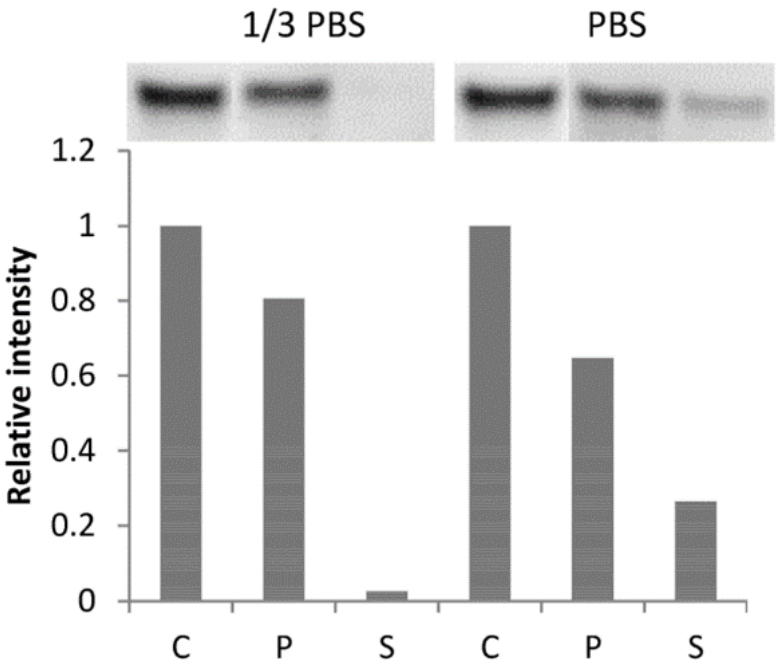

Figure 2. Binding of MIP-2 (200 ng/ml) with RB MPs (10% wet *v/v*) in PBS and three-fold diluted PBS at 4°C overnight.
The graph shows the relative intensities of the above Western blot band intensities of the control CK (C), CK eluted from the MPs (P), and CK unbound in the supernatant (S).

The band intensities of the eluted CK relative to the total amount initially loaded were approximately 80% in diluted PBS, and 70% in 1x PBS, confirming that the disappearance of CK from the supernatant was due to capture by the MPs. In both buffer conditions the total signal intensity of the particle eluate and the supernatant fractions did not equal that of the control. It is likely that some aggregation of the CK in these solutions, which lacked a carrier protein, may have occurred and the resulting dimers or multimers were not detected. Additionally, some of the CK may have remained strongly bound to the MPs and this interaction was not broken during elution.

MP interactions with CKs are driven by mass law equilibrium binding

To determine the affinities of MPs for CKs, we measured the ability of different concentrations of MPs to capture CK. Dilutions of CB and RB MPs were incubated with either IL-8 (250 pg/ml) or MCP-1 (1 ng/ml). The unbound CK in the supernatant was measured by ELISA after overnight incubation. Expectedly, solutions containing higher concentrations of MPs bound more CK. The calculations of dissociation equilibrium constants (K_d) were made with a few assumptions: (1) the fraction of CK bound to MPs was linear across all MP dilutions and (2) the CKs were able to independently bind to equal numbers of binding sites on each type of MP. The basis for these assumptions is that the amount of AA in MPs for dye coupling was calculated to be approximately 40 µM, while the greatest amount of CK used in these experiments was 0.1 µM. Therefore, the CK binding sites within the dye-coupled MPs were not saturated and did not interfere with each other within the range of CK concentrations tested here. To calculate the K_d, the standard equilibrium equation was used:

Equation 1: Standard Equilibrium Equation

$K_d = [F][P]/[B]$

where [F] and [B] represent the concentrations of free and MP-bound CKs, respectively, and [P] represents the concentration of available CK binding sites on the MPs. By rearranging this equation and plotting [B]/[F] *vs*. the MP dilution, K_d is easily calculated from the slope of the resulting line of best fit (Figure 3). These K_d values were calculated to be in the range of low micromolar to high nanomolar. This supports the hypothesis that these MPs could be used to achieve sustained release of CK. Our MP-CK affinities are similar to those seen in other nanoparticle-mediated delivery systems[45,46].

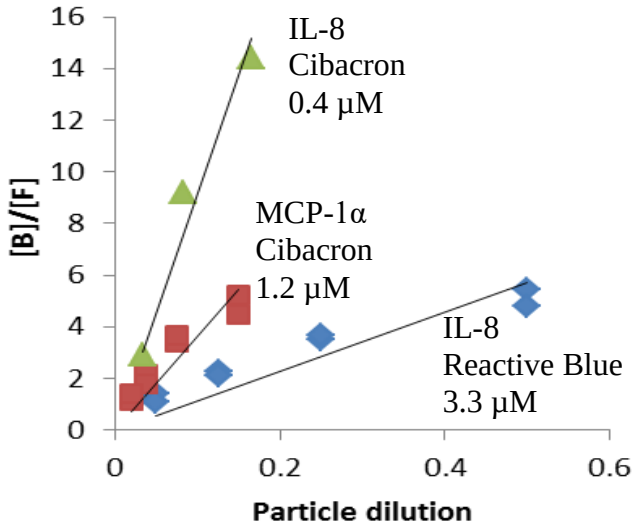

Figure 3. Binding isotherms depicting dissociation equilibrium constants (K_d values) for multiple CK-MP pairs. Dilutions of CB or RB MPs from a 5% wet *v/v* suspension were incubated with IL-8 (0.25 ng/ml) or MCP-1 (1 ng/ml) in PBS at 4°C overnight. [F] and [B] represent the concentrations of free and MP-bound CKs, respectively.

MPs provide sustained release of their CK cargo in a temperature-dependent, BSA-independent manner

After determining the K_d values for a few MP-CK pairs, we wanted to further assess the kinetics of CK release. Suspensions of RB or CB MPs loaded with MIP-2 or IL-8 CKs in 1/3 PBS (high-binding conditions) were assessed for their CK release rates at 22°C and at 37°C (Figure 4A-B). After overnight incubation at 4°C to load the MPs with CK, the MPs were then briefly washed and re-suspended in a much larger volume of buffer to promote CK dissociation. Aliquots of these suspensions were taken at the several times following resuspension, centrifuged, MP pellets were boiled with SDS and DTT for elution, and then the eluted material was used for Western blot analysis, and the intensity of the bands were quantified. In all cases, there was expectedly little detectable CK remaining in the supernatant after overnight incubation. Additionally, the gradual decrease in band intensity of the eluates indicated successful CK release, as the amount of CK bound to the MPs decreased over time. Dissociation of CK occurred more rapidly at 37°C than at 22°C. Interestingly, this contradicts other studies on drug or biomolecule release from thermoresponsive hydrogel delivery vehicles, which have reported longer times required for release at higher temperatures as the structural shrinkage was suggested to entrap the cargo inside the hydrogel[47]. In our study, it appears that the diffusion of dissociated CK from MPs was not impeded by higher temperatures.

The amount of CK detected immediately after a brief wash and resuspension appeared less in all cases than the expected amount in the control wells. The initial loss of band intensity likely represents a fraction of CK which was loosely associated with the MPs during the binding step, and subsequently lost during the wash. This resembles the

phenomenon of "burst release" which has been observed frequently in controlled release studies from other types of delivery vehicles, where a rapid initial small bolus release occurs before achieving first-order kinetics[48,49]. Sustained topical antibiotic therapies have utilized this as an advantage for the prevention of systemic spread of bacteria from a wound site[50], so this should not be immediately considered as an indication against the potential utility of our MP technique. The remaining CK from our MPs demonstrated a pattern of sustained release with rates dependent on temperature and the particular CK-MP pair tested.

We additionally examined the role of bovine serum albumin (BSA) on CK binding and release, predicting that it could interfere with both steps. BSA is a globular carrier protein that is frequently used as an additive in solutions at concentrations up to 10 mg/ml for protein stabilization and preventing aggregation. As such, BSA is known to bind many proteins[51] and dyes including CB with high affinity[52], and is estimated to have a strong positive charge of 10 at physiological pH[53]. We measured the amount of CK loaded and released from CB MPs in 1/3 PBS containing BSA at concentrations of 0, 1, or 10 mg/ml (Figure 4C) and found that BSA did not significantly influence the loading step, as the BSA protein is larger than the exclusion size of our MPs. Similarly, the presence of BSA in the resuspension buffer did not significantly influence the amount of MIP-2 released from MPs.

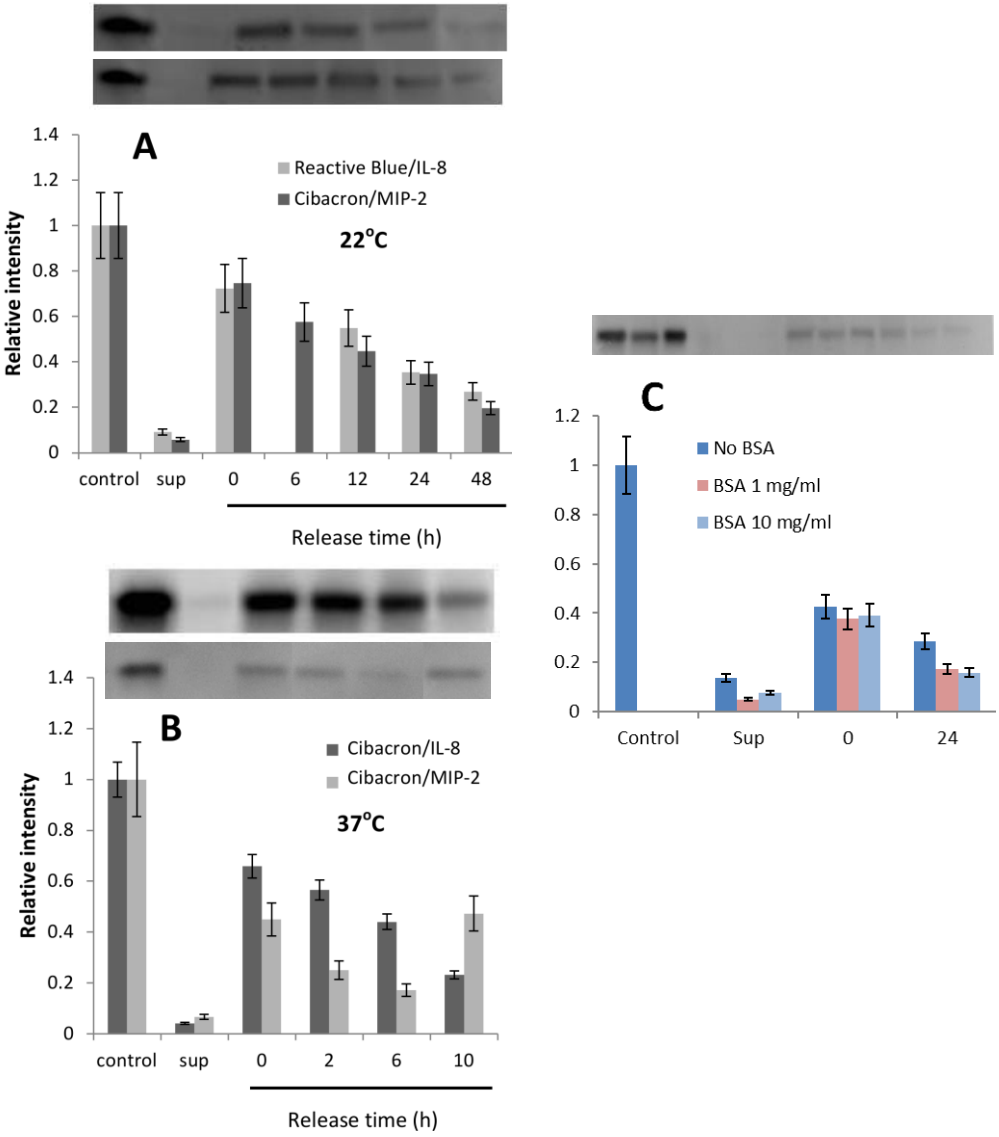

Figure 4. Quantification of the CK band intensities from the Western blots (shown on top of respective graphs) relative to corresponding controls.
CKs (2 µg/ml) were loaded onto 10% wet *v/v* MP suspensions in 100 µl total volume of 1/3 PBS at 4°C overnight. After overnight incubation, the MPs were pelleted, supernatants were removed, and the MP pellets were washed briefly and re-suspended in 1 ml of the indicated buffers. (A) CK release at 22°C for RB loaded with IL-8 (top band; 6 h not done) and CB loaded with MIP-2 (bottom band); (B) CK release at 37°C into buffer containing 1 mg/ml BSA for CB loaded separately with IL-8 (top band) and MIP-2 (bottom band); (C) MIP-2 binding and release from CB in 1/3 PBS containing 0, 1, or 10 mg/ml BSA. Error bars indicate 95% confidence intervals.

The relative band intensities from the Western blots quantitated by Figure 4A-B of remaining bound CK content after resuspension were used to calculate the kinetic dissociation constants (k_d) and the half-lives ($t_{1/2}$) of the CK-MP complexes (Table 1). The rate equation for first-order kinetics is:

Equation 2: Rate equation for first-order kinetics

$$[B] = [B_0]e^{-kt}$$

in which B is the amount of reactant (CK-MP complex) present initially and at time *t*. Rearranging this equation yields:

$$k_d = \ln([B_0]/[B])/t$$

to determine the kinetic dissociation constant. The half-life of first-order rate equations can then be calculated as:

Equation 3: Half-life of first-order rate equations

$$t_{1/2} = \ln 2/k_d$$

giving an approximation for the time required for half of the bound CK to be released by the MPs. Pharmacological studies typically assume that the amount of activity or release after five half-lives (3.125% from initial amount) is considered negligible. Therefore, according to Table 1, sustained CK release from MPs in physiological conditions (37°C) would expectedly occur for more than 20 h, which seems to be sufficient for the sustained immune cell chemotaxis. Additionally, the activation energies of dissociation for both CKs were found to be similar using the Arrhenius Law given by the equation:

Equation 4: Arrhenius Law Equation

$$\ln k = \ln A - E_a/RT$$

The activation energy (E_a) was calculated from the slope of the line ($m = -E_a/R$) on a graph of ln*k vs.* 1/T using the k_d values from Table 1, where T is the temperature and R is the universal gas constant. Assuming slight variations in ambient room temperature ranging between 18-24°C, the activation energies of CK release from CB MPs were estimated to be between 70-104 and 68-102 kJ/mol respectively for IL-8 and MIP-2, similar to biologically-relevant reactions. Our results indicate that the structural changes in the MPs caused by the temperature shift did not impose considerable constraints on the dissociation of CKs.

Table 1. Kinetic dissociation constants (k_d) and half-life times in PBS for release of IL-8 and MIP-2 from CB and RB MPs.

	22ºC		37°C	
Bait	**IL-8**	**MIP-2**	**IL-8**	**MIP-2**
CB	k_d 0.016±0.005* h^{-1} $t_{1/2}$ 43.5 h	k_d 0.030±0.002* h^{-1} $t_{1/2}$ 23.7 h	k_d 0.094±0.017* h^{-1} $t_{1/2}$ 7.44 h (BSA 1 mg/mL)***	k_d 0.17±0.05* h^{-1} $t_{1/2}$ 4.1 h (BSA 1 mg/mL)***
RB	k_d 0.022±0.004* h^{-1} $t_{1/2}$ 31.3 h	ND**	ND**	ND**

* Standard deviations of k_d calculated from linear approximations of the kinetic curves; ** Not determined; *** BSA was included in the dissociation buffer.

CKs released from MPs retain their chemotactic activity in *in vitro* cell migration assays

Our kinetic studies demonstrated that the MPs are successfully able to release CKs after binding with half-lives of several hours upon re-equilibriation. Here we tested if the functionality of the released CKs was retained by measuring their chemoattractant activity in a Boyden-type transwell assay. MPs were pelleted after being loaded with CKs at 4°C overnight, re-suspended in a fresh volume of CSFM, and incubated at 37°C for 3 h to allow CK dissociation. The MPs were pelleted again after incubation and the supernatant containing the released CK was transferred into the bottom chambers of transwell plates loaded with serum-starved monocytic THP-1 or U937 cells in the top chambers. The plates were incubated for 4 h to allow cell migration.

THP-1 cells were highly responsive to the MIP-1α released from MPs (Figure 5). Similar activity was seen with U937 cells (but not THP-1 cells) in response to IL-8 (not shown). A freshly prepared MIP-1α calibration curve displayed typical dose-dependent response with the highest activity occurring in response to 10-30 ng/ml CK. Given the off-rate for MPs paired with IL-8 is roughly 7.4 h, incubation for 3 h is estimated to dissociate approximately 25% of the bound CK. Thus as expected, the CK loaded onto MPs and partially released before the assay demonstrated only a fraction of the total chemotactic activity which would be present in the case of complete CK release. When plotted against the estimated amount released, the chemotactic activity of MIP-1α overlapped with the standard curve, indicating no substantial loss of the CK activity due to the MP binding and release. In comparison, MIP-1α incubated without MPs in the

conditions of CK loading lost a substantial part of its activity, likely due to its instability and aggregation in a diluted solution[54].

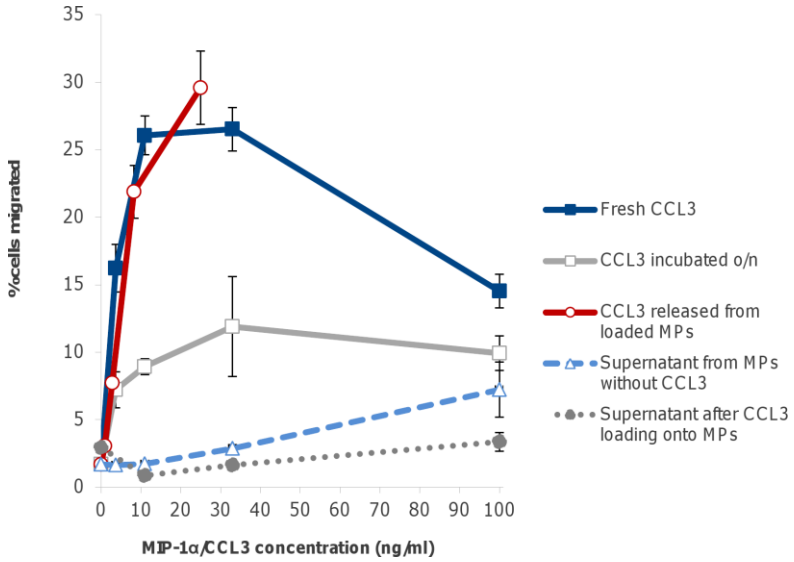

Figure 5. Chemotactic activity of MIP-1α after release from MPs with THP-1 cells in a transwell format. MP-bound MIP-1α was assayed after its release from MPs in CSFM at 37°C for 3 h. The MPs were removed by centrifugation and the supernatants containing released CK were transferred into bottom wells of the transwell plate. Serum-starved cells in CSFM were added to the top chambers. Cell migration to the bottom chamber was enumerated after incubation for 4 h at 37°C, 5% CO_2. Values on the x-axis correspond to the concentrations calculated from the total amount of MIP-1α used to prepare solutions (solid lines with open and closed squares) or the estimated amount of MIP-1α released from the MPs during 3-h incubation (solid line with open circles). Dashed line represents the chemotactic activity of supernatants after the control incubations of MPs without MIP-1α in the amounts used for the standard curve. Dotted line corresponds to the chemotactic activity left in solution after MPs were loaded with the indicated concentrations of MIP-1α. Error bars indicate 95% confidence intervals.

AIM II

MPs are not directly toxic to cultured Raw 264.7 cells

As a preliminary assessment of safety prior to administration in animals, the cytotoxicity of MPs on host cells was measured *in vitro*. Mouse Raw 264.7 cells were chosen because the MPs are likely to become engulfed by phagocytic cells, and because these macrophages are a model cell line used frequently in MP toxicity analyses[55–57]. The cultured cells were exposed to MPs and cell viability was measured as the ability of cells to reduce Alamar Blue dye (resazurin). Since the MPs contain coupled CB dye, additional control cultures included the soluble CB dye at concentration corresponding to its content in the MPs (diluted to the concentration of allylamine used in the MP polymerization procedure for introducing primary amino groups into their content for CB coupling). The active chlorine of the reactive dye was preliminarily hydrolyzed during incubation in the 0.1 M carbonate buffer, similar to its removal in the particle-coupling process. There was no measurable toxicity observed after 24-h exposure to any of the MPs at concentrations up to 10% pellet volume or to the soluble CB dye of similar concentration (Figure 6). Higher CB dye concentrations however showed partial cytotoxicity which occurred in a dose-dependent manner.

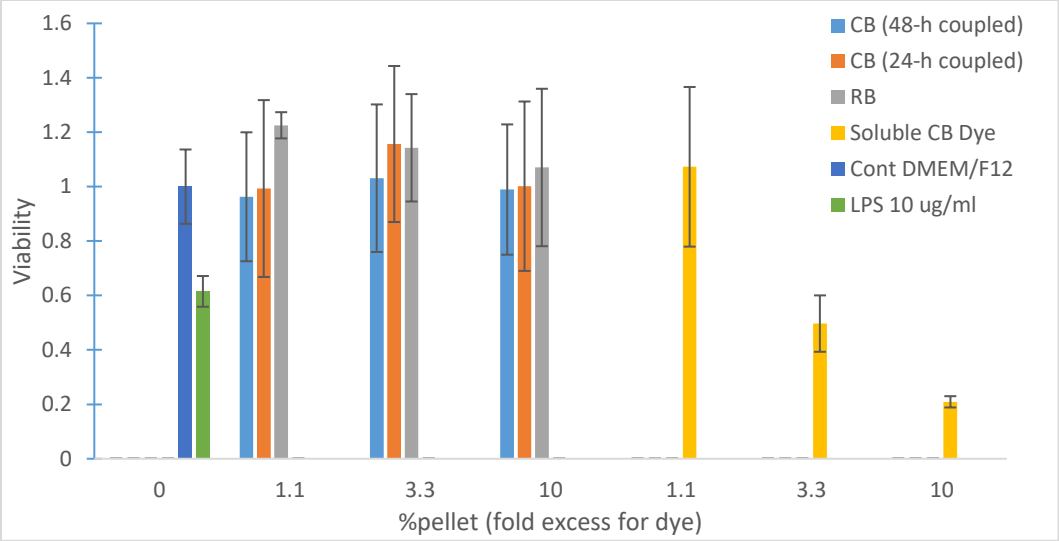

Figure 6. Viability of Raw 264.7 macrophages upon exposure to MPs and soluble CB dye.
Raw 264.7 cells were grown to 60-70% confluency in a 96-well plate, then serum-starved for 1 h and exposed to CB or Reactive Blue (RB) MPs or soluble CB dye diluted in serum-free DMEM/F12 medium for 24 h. The CB MPs included were coupled with the dye for either 48 h or 24 h, as indicated. The ability of cells to reduce Alamar Blue dye was used as a measure of cell viability after the 24-h incubation. Error bare indicate 95% confidence intervals.

Subcutaneous injection quickly delivers MPs to regional LNs

We next characterized the behavior of MPs *in vivo* through visualization of their sites of accumulation after injection and their ability to manipulate immune cell trafficking. First, MPs functionalized with allylamine were labelled through the coupling of a fluorescent dye, Alexa Fluor 555 so they could be visualized in excised tissue. This model of injection was chosen because the patterns of lymphatic drainage were previously characterized[58]. The labelled MPs were subcutaneously injected into the hind footpads (FPs) of mice, where they were expected to enter the lymphatics and be carried to the popliteal and inguinal LNs. Lymph drainage from the hind legs in mice enters the popliteal and inguinal LNs approximately evenly so these were chosen for histological examination.

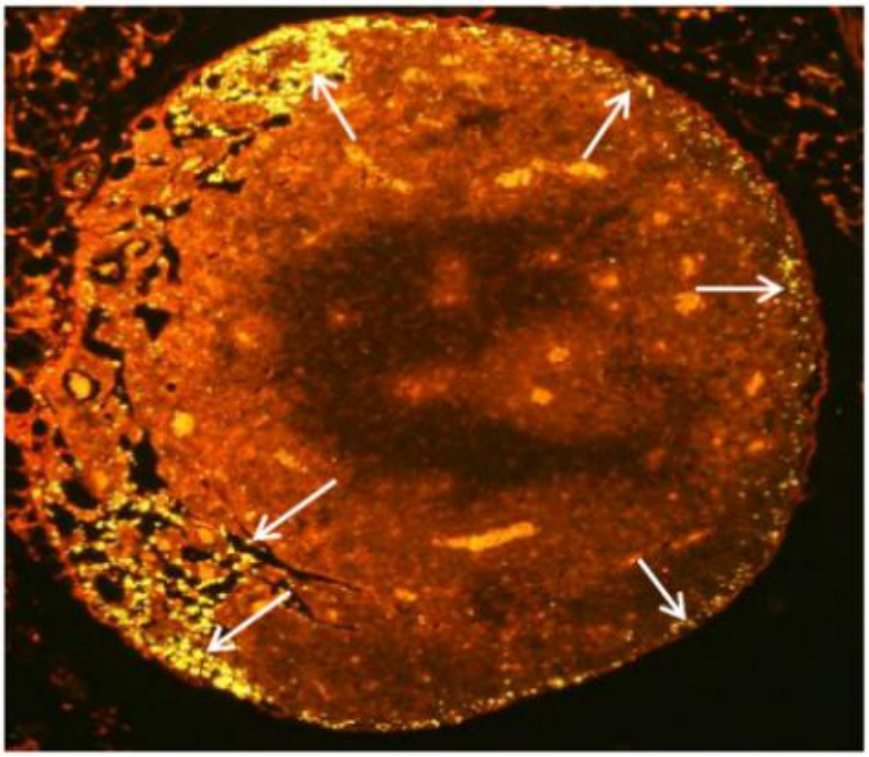

Figure 7. Fluorescently-labelled MPs are quickly carried to the popliteal (shown) and inguinal (not shown) LNs when injected into the hind FPs of mice.
Alexa Fluor 555-labelled MPs suspended in PBS (20 µL) were injected into the mouse hind FPs, and the regional popliteal and inguinal LNs were removed after 30 min for histological examination. Arrows indicate the bright yellow MPs accumulated in the subcapsular and medullary regions.

Within the LN, lymph flow first enters on the convex side through afferent lymphatic vessels into the subcapsular sinuses, then through the trabecular sinuses, and finally through the medullary sinuses. The medullary sinuses have a smaller diameter than earlier sinuses, allowing large cells like macrophages to be retained here. Passage through the medullary sinuses leads to exit from the LN *via* efferent vessels at the hilum on the concave side[59,60].

As expected, the MPs were detected as bright yellow dots in the popliteal and inguinal LNs, primarily in the subcapsular and medullary regions as early as 30 min after injection (Figure 7). The popliteal LN shown is representative of results seen in both types of LN. Within the LN, the localization of MPs in the subcapsular and medullary sinuses is favorable for their interaction with macrophages and DCs. A portion of MPs was also found un-migrated in the FP visible as a blue smear under the skin. Previous studies have suggested that MPs larger than 500 nm migrate poorly through the lymphatics, but can become phagocytosed by tissue-resident macrophages and DCs which migrate to the draining LN[61]. It is likely that the difference between the numbers of MPs in the FPs *vs*. the LNs would become less during the following time, as more MPs would be gradually phagocytosed by resident phagocytes and carried to the LN.

CK-MPs enhance mobilization of immune cells to the LNs upon administration in mice

Knowing that a portion of the injected MPs accumulate in the regional LNs, we next examined the immune response to MPs injected by this mode. Animals were sacrificed shortly after receiving hind FP injections of control "empty" RB MPs which did not contain loaded CK. The popliteal LNs were immunohistochemically stained for neutrophils and counterstained with hematoxylin. Infiltrated neutrophils were detected using an antibody against myeloperoxidase, a potent antimicrobial enzyme produced in their cytoplasmic granules. Empty MPs induced low levels of neutrophil infiltration which was slightly more detectable at 4 h than at 30 min (Figure 8), and subsided at 24 h (not shown). The detected neutrophils were primarily located in the subcapsular and

medullary regions, in agreement with the fluorescently-labelled MPs which were shown to accumulate there. Therefore, it is likely that the empty MPs induced a slight response by neutrophils, and that those responding were present from nearby circulation. The LPS endotoxin content within the MPs was not taken into consideration for this experiment, but was measured and adjusted in later experiments involving prolonged survival analysis. Of note, the MPs injected here contained approximately 2.5 EU/ml endotoxin, but did not induce a large or prolonged immune response. The numbers of neutrophils present were quantified and are included in Figure 10. The highest detection of neutrophils in response to empty MPs was at 4 h, and was averaged to be 5.9±2.4 per field of view under 100x magnification in the subcapsular region, and 10.9±4.6 in the medullary region. The levels of infiltrated neutrophils counted at 24 h were less than 2 and 5 per field of view in the subcapsular and medullary regions, respectively, at both 30 min and 24 h.

Empty MPs appeared to induce minimal neutrophil response, so the contributions of CKs were measured. For this purpose, mice received 50 µl injections in each hind FP of either soluble or MP-bound CK. A mixture of the neutrophil-attracting CKs IL-8 and MIP-1α (doses of each were 1 µg/ml or 0.1 µg/ml) were injected in PBS or in PBS containing 5% suspension of RB MPs after overnight loading. LNs stained for neutrophil myeloperoxidase activity in response to soluble CK or MP-bound CK are shown in Figure 9, and the neutrophil counts per field of view are quantified in Figure 10.

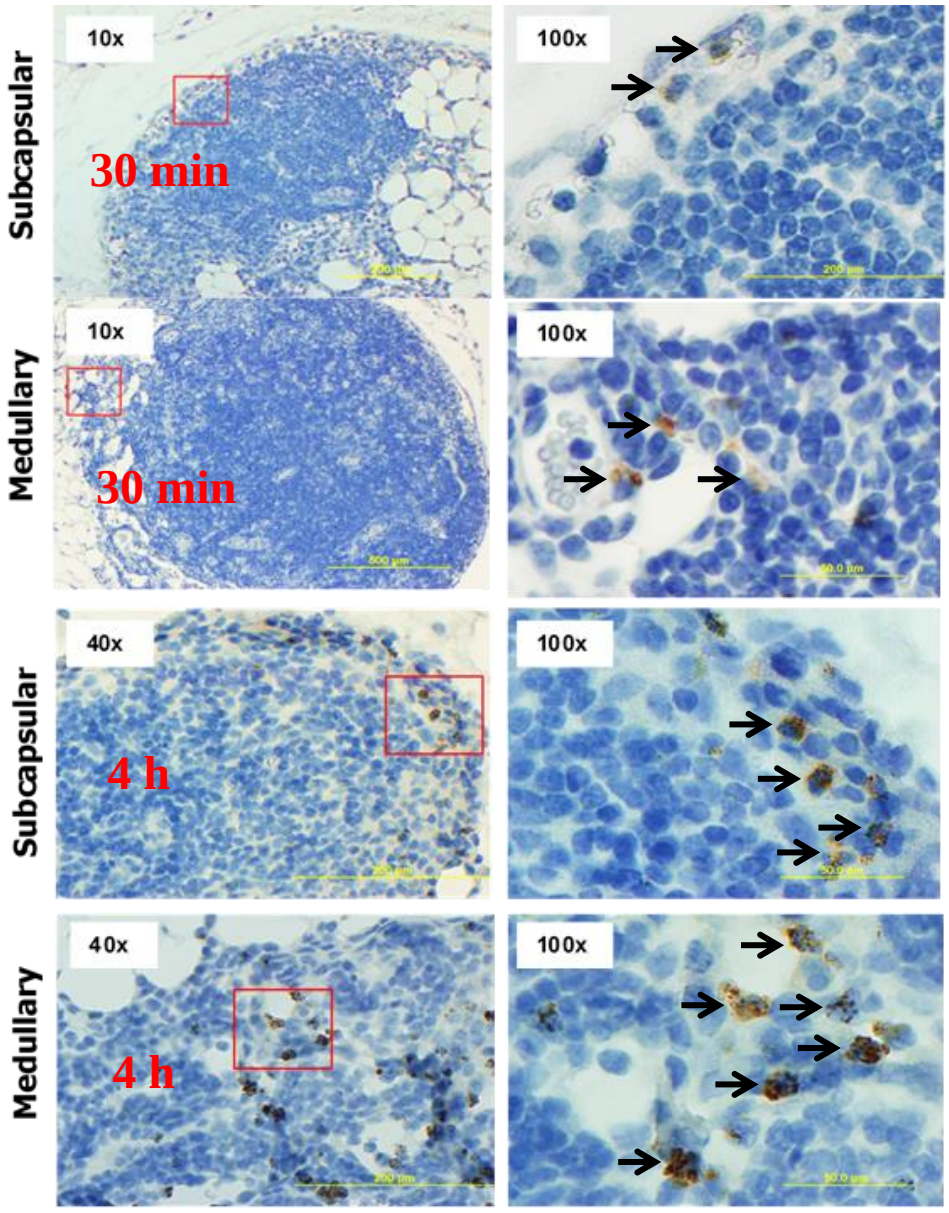

Figure 8. Representative images of the subcapsular and medullary regions of popliteal LNs after FP injection with empty RB MPs.
Mice were injected with RB MPs (5% wet *v/v*, 50 µl) without loaded CK. At multiple times post-injection, animals were sacrificed and LNs were taken for immunohistochemical staining. Tissues were stained with myeloperoxidase and counterstained with hematoxylin to detect neutrophils. The squared regions in the left panel are shown at higher magnification on the right.

Injection with soluble CKs induced dose-dependent neutrophil migration which was generally intermediate between the empty MPs and the CK-MPs, visualized at both 4 h and 24 h (Figures 9, 10). Soluble CKs induced the highest neutrophil response at 4 h in both subcapsular and medullary regions, which dropped significantly at 24 h. This drop predictably occurred because the bolus of CK concentration dissipated over the 24-h period, so the immune response that was present at 4 h subsided. Comparatively, injection with CK-MPs induced the highest neutrophil response, and was generally greater at 24 h rather than 4 h. This agrees with the calculated release rates for multiple CK-MP pairs, which were expected to maintain biologically significant CK release for over 20 h. The sustained release from the MPs allowed the CK concentration gradient to be maintained for longer, which induced continued neutrophil migration into the tissue.

Due to the size characteristics of the subcapsular and medullary regions, a strict comparison between the number of neutrophils in each region is not possible. Under 100x magnification, the medullary region for most LN slices encompasses most of the field of view. The subcapsular region at the same magnification only spans a thin layer below the periphery of the tissue. Therefore, the subcapsular region was generally less responsive to changes in neutrophil numbers when comparing those from mice injected with the same concentration of soluble or MP-bound CK. The larger medullary region displayed greater sensitivity to the influence of CK dose and the nature of the CK injected (soluble or MP-bound). The subcapsular region is also limited in where it can receive migrating immune cells from. Lymph flow through the LN is unidirectional, so immune cells present in the subcapsular region can only arrive there through the afferent lymphatic vessels. In

contrast, the medullary region is capable of receiving cells from the bloodstream, which enter into the LN through migration *via* high endothelial venules (HEVs)[62]. The higher counts in the medullary region in response to CK-MPs therefore likely reflect neutrophils entering the LN from HEVs and flowing through to this site of MP accumulation.

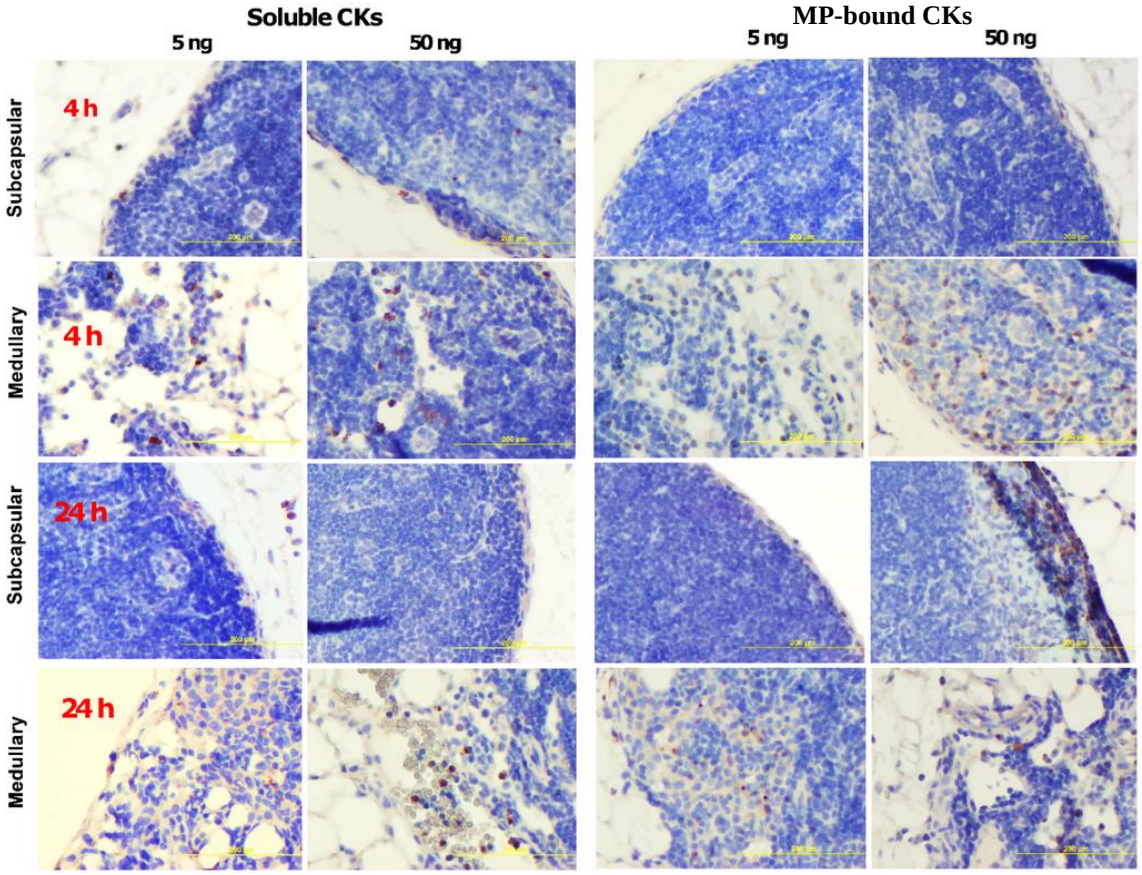

Figure 9. Representative images of the subcapsular and medullary regions of popliteal LNs after FP injection soluble or MP-bound CKs.
CKs were loaded onto RB MPs (5% wet *v*/v suspension) overnight at 4°C. Mice were subcutaneously administered 50 µl of soluble or MP-bound CKs (1 µg/ml or 0.1 µg/ml of each MIP-1α and IL-8) in PBS. Tissues were taken at 4 h or 24 h post-injection, stained with myeloperoxidase, and counterstained with hematoxylin to measure neutrophil infiltration.

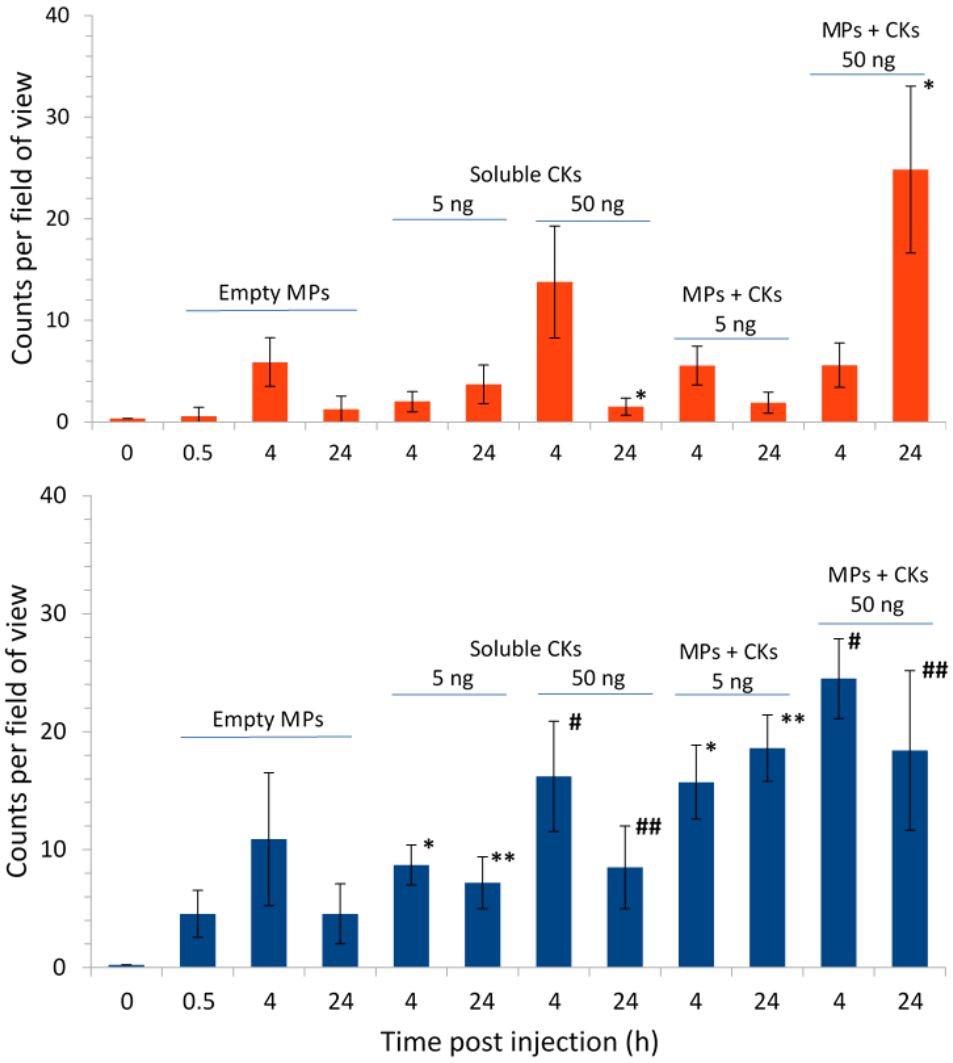

Figure 10. Enumeration of neutrophil counts in the subcapsular (A) and medullary (B) regions of popliteal LNs from the experiments shown in Figures 8 and 9.
Mice received injections of soluble or RB MP-loaded IL-8 and MIP-1α into both hind FPs. The number of cells stained positive for myeloperoxidase activity were counted from five randomly selected fields of view (0.002 mm^2 each) from each region at 100x magnification. Error bars correspond to 95% confidence intervals. * and # indicate $p \leq 0.05$ between the corresponding counts with and without MPs.

AIM III

MPs influence the inflammatory response at the site of *B. anthracis* infection and improve the survival of spore-challenged mice

After characterizing the behavior of our CK-MPs *in vivo*, we further hypothesized that their administration could be protective in animals challenged with an infectious agent. We chose *B. anthracis* Sterne 34F2 spores as our infectious agent, which was subcutaneously injected into the FPs similarly to MPs. In this model the injected spores may proliferate at this site or enter the lymphatics where they are quickly phagocytosed by macrophages and DCs and delivered to the regional LNs[63]. The anthrax infectious process involves characteristic immunosuppression, so we hypothesized that the co-localization of CK-MPs and spores along the same route would promote host survival. Our MPs would predictably stimulate neutrophil recruitment to the site of infection and regional LNs prior to bacterial accumulation and germination, and thereby overcome the suppression of chemotactic migration normally induced by the bacterium.

Six groups of mice (n= 8-9 each) were challenged in both hind FPs with $2.6x10^6$ *B. anthracis* Sterne 34F2 spores in a 50 µl volume, with or without treatment with MPs and/or CKs. This experiment was carried out with a batch of CB MPs virtually free from LPS contamination (0.14 EU/ml of MP suspension). Group 1 served as the infection-only control group. Group 2 was injected with empty MPs 24 h prior to infection, and twice post-infection at 4 h and 24 h. Group 3 was similarly injected three times, but instead

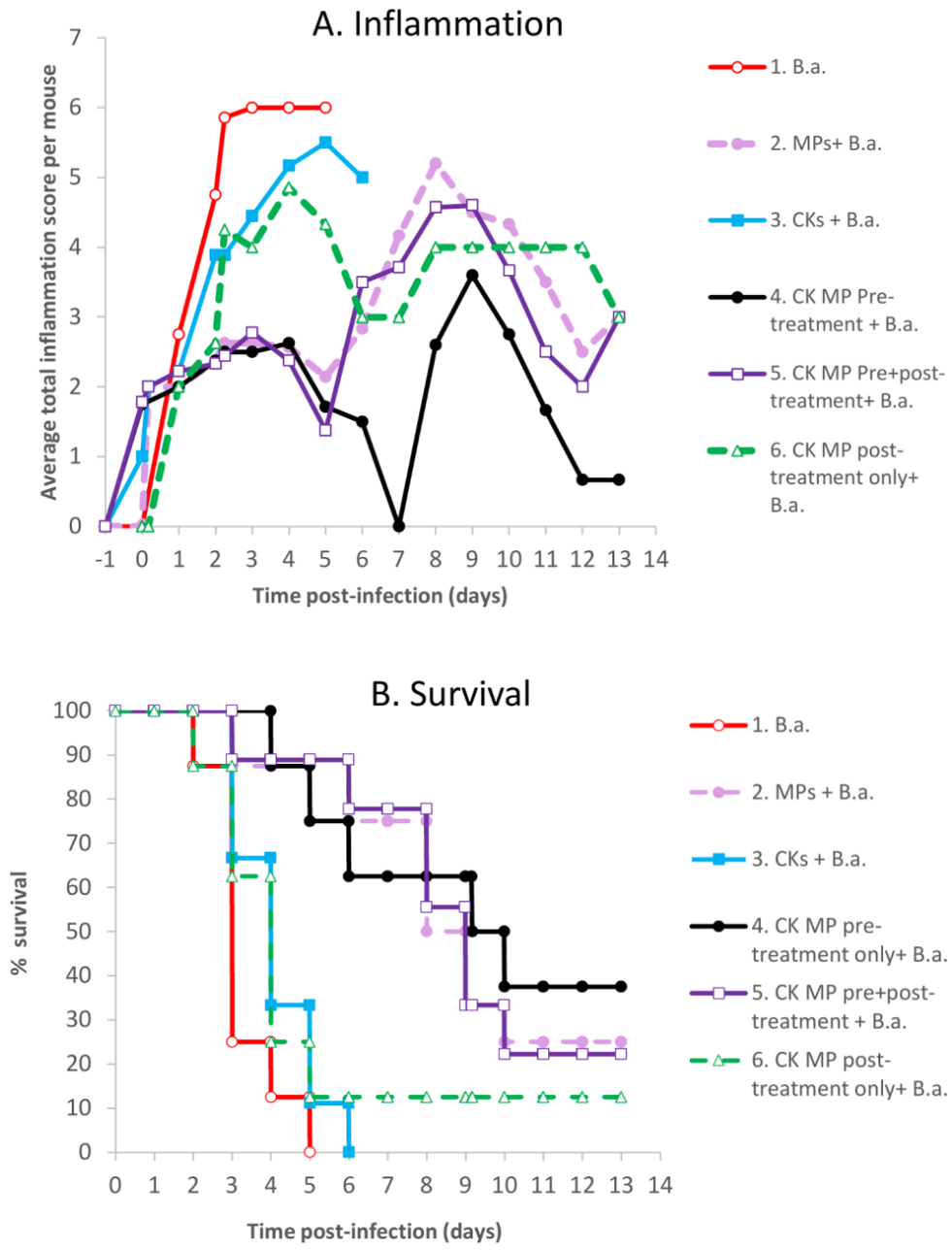

Figure 11. Administration of MPs and/or CK influences (A) total inflammation seen in both hind FPs and (B) survival in anthrax spore-challenged mice.
Six groups of mice (n= 8-9 mice per group) were challenged with $2.6x10^6$ spores in a 50 µl dose into each hind FP. Group 1 was the untreated, infection only control. Groups 2 and 3 each received one prophylactic dose and two post-infection doses (at 4 h and 24 h) of either empty MPs (10% wet *v*/v) or soluble CKs (1 µg/ml each of IL-8 and MIP-1α). Groups 4, 5, and 6 received doses of CK-MPs administered either prophylactically only, both prophylactically and post-infection, or post-infection only, respectively. All injections were subcutaneously administered as 50 µl into both hind FPs.

with soluble CK (1 μg/ml each of IL-8 and MIP-1α). Groups 4, 5, and 6 received injections of CK-MPs either prophylactically only, both prophylactically and twice post-infection, or twice post-infection only, respectively. The mice were inspected daily for two weeks and were assigned semi-quantitative scores for the inflammation seen in each hind FP as defined in the "Research Design" section. This system of inflammation scoring is similar to others which have been used to characterize mice challenged with an infectious agent[64]. The statistical significance ($\alpha = 0.05$) of the total inflammation scores per mouse was determined using a two-tailed Mann-Whitney U test. Mortality curves were compared using the Log Rank Test.

All mice in Group 1 developed high levels of inflammation and died within five days (Figure 11). Groups 3 and 6 were statistically similar to Group 1 for both inflammation and survival. All mice in these groups (except one mouse in Group 6) displayed high levels of inflammation, which correlated with rapid death by day 6. In contrast, Groups 2, 4, and 5 demonstrated significantly reduced levels of inflammation (p values in the range from 0.001 to 0.008) and survival ($p<0.0007$, Log-Rank test). Up to 35% of the mice from these groups were surviving at the end of the two-week infection period. Group 4 appeared to have the greatest improvements in reduced inflammation and increased survival, but was not statistically different from Groups 2 and 5. These three groups also appeared to develop inflammation which occurred in two phases in which the initial inflammatory response became reduced to reach minimal levels, then increased, and then reduced again. Both peaks and regressions were only significant in Group 4 ($p< 0.01$) and in Group 5 for the second phase only ($p< 0.03$). Surprisingly, the mice in

Group 6 which received CK-MPs injected twice after infection were not statistically different from the untreated mice in Group 1. It appears that administration of therapy prior to or immediately after is critical in cases of anthrax infection, as the rapid uptake of spores by macrophages and subsequent germination is sufficient to turn the odds of survival in favor of the bacteria instead of the host. Treatment with CK-MPs after infection was likely unable to overcome the suppression of neutrophil migration induced by the bacteria.

In all the groups described in Figure 11, the deaths which occurred took place predominantly in mice with high inflammatory scores (Figure 12). Death in any group only occurred in animals which demonstrated total inflammation per mouse ≥ 3, but not all animals with high inflammation succumbed to infection.

An independent replicate experiment was performed to evaluate the importance of pre-treatment duration before infection. Group 1 (*B. anthracis*) and Group 4 (24-h pre-treatment plus *B. anthracis*) from the experiment shown in Figure 11 were replicated and challenged with 8×10^6 spores/mouse. We also included an additional group which received CK-MP pre-treatment merely 4 h prior to infection. At day 13 p.i., 50% and 70% of animals survived in the 4-h and 24-h pre-treated groups, respectively (not shown). Both pre-treated groups demonstrated significantly ($\alpha=0.01$) decreased levels of inflammation compared to the control group at days 1 and 2 which presented in a bi-phasic manner as before. The Log-Rank test showed that all three groups which received only pre-treatment (at 4-h or 24-h) did not statistically differ from each other ($p<0.21$) with an average survival of 53±16% (SD).

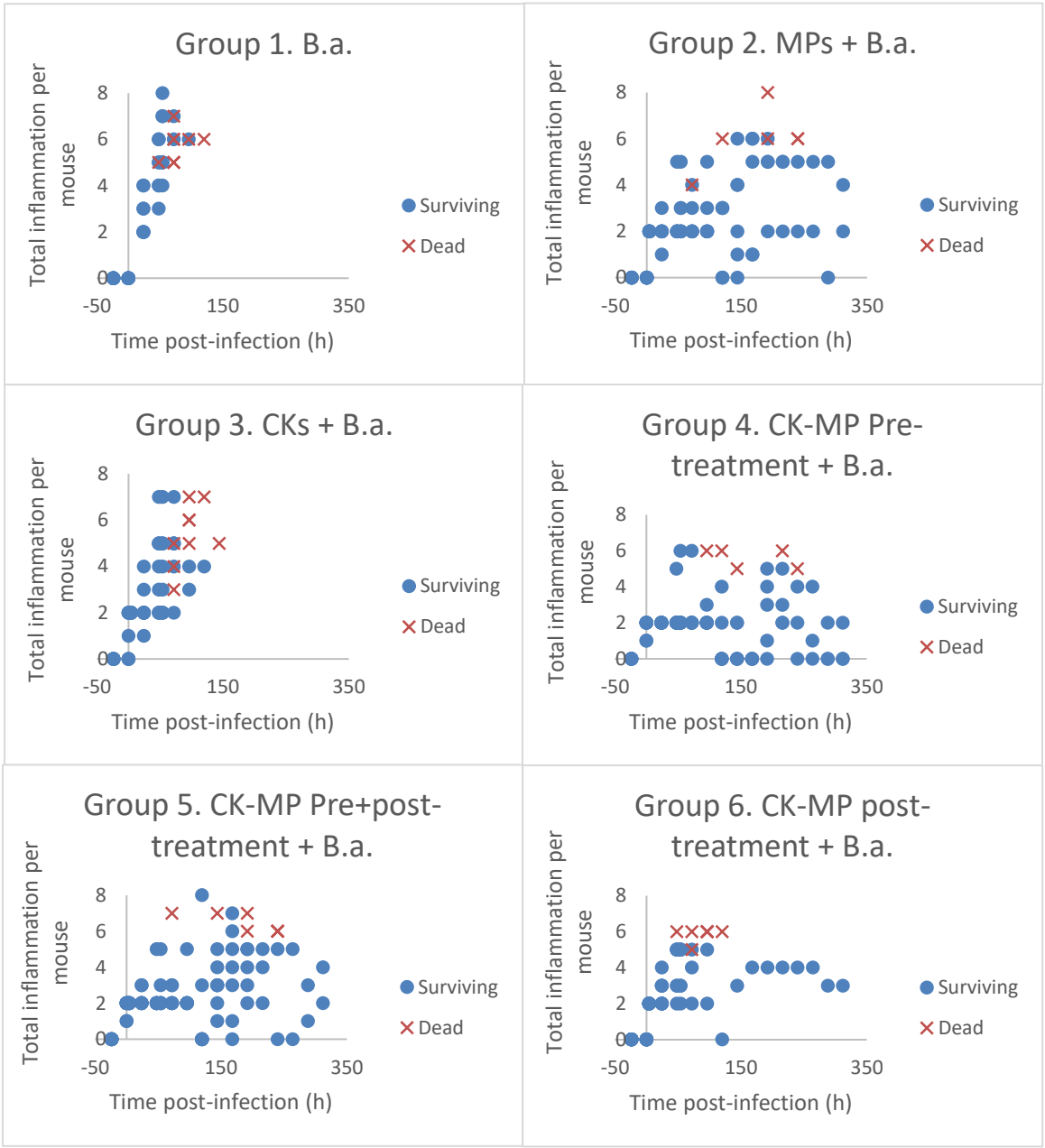

Figure 12. Mice that succumbed to infection (from the experiment shown in Figure 11) displayed elevated levels of footpad inflammation.
Each data point indicates the total inflammation score for one or several mice with the same score at the indicated observation time. Higher inflammation scores were not a direct predictor of mortality as some mice demonstrated greater inflammation and survived or died at a later time, but all mice which died in any group demonstrated increased inflammation.

Both the MPs and CK-MPs contribute to the protection of mice against anthrax

To address the unexpected result of empty MPs appearing statistically as protective as CK-loaded ones, we estimated the LD_{50} of *B. anthracis* spores injected in this model. This was determined to be $4.3x10^4$ spores per mouse. It can thus be assumed that the injection of at least $5.2x10^6$ spores per mouse (more than 100 LD_{50}s) in our previous experiments masked the individual contributions of each the MP and the loaded CK. Therefore, we repeated the experiment in which some animals received pre-treatment injections of MPs or CK-MPs prior to infection, but this time using multiple reduced spore challenge doses. A clear discrimination between the groups treated with MPs and CK-MPs became apparent (Figure 13).

Animals received 50 µl of high, middle, or low challenge doses containing $2.9x10^6$, $9.7x10^5$, or $3.2x10^5$ spores/ml, respectively, into each hind FP. The low dose (equivalent to 0.7 LD_{50}s per mouse) resulted in only a minor decrease in survival in all groups, including the control group which was not pre-treated, by the end of the two-week period and therefore could not be used to discern the contribution of loaded CKs. Control groups receiving the high (7 LD_{50}s) and middle (2 LD_{50}s) doses in comparison resulted in either the death of all mice or all but one mouse, respectively, within the first week. Groups receiving MPs or CK-MPs prior to challenge with the middle and high doses of spores demonstrated statistically improved survival (p values<0.0001). The overall survival at the end of the two-week period was statistically similar between these pre-treated groups, but the onset of mortality was delayed in animals pre-treated with CK-MPs. Animals challenged with the high dose of spores reached 25% mortality by day

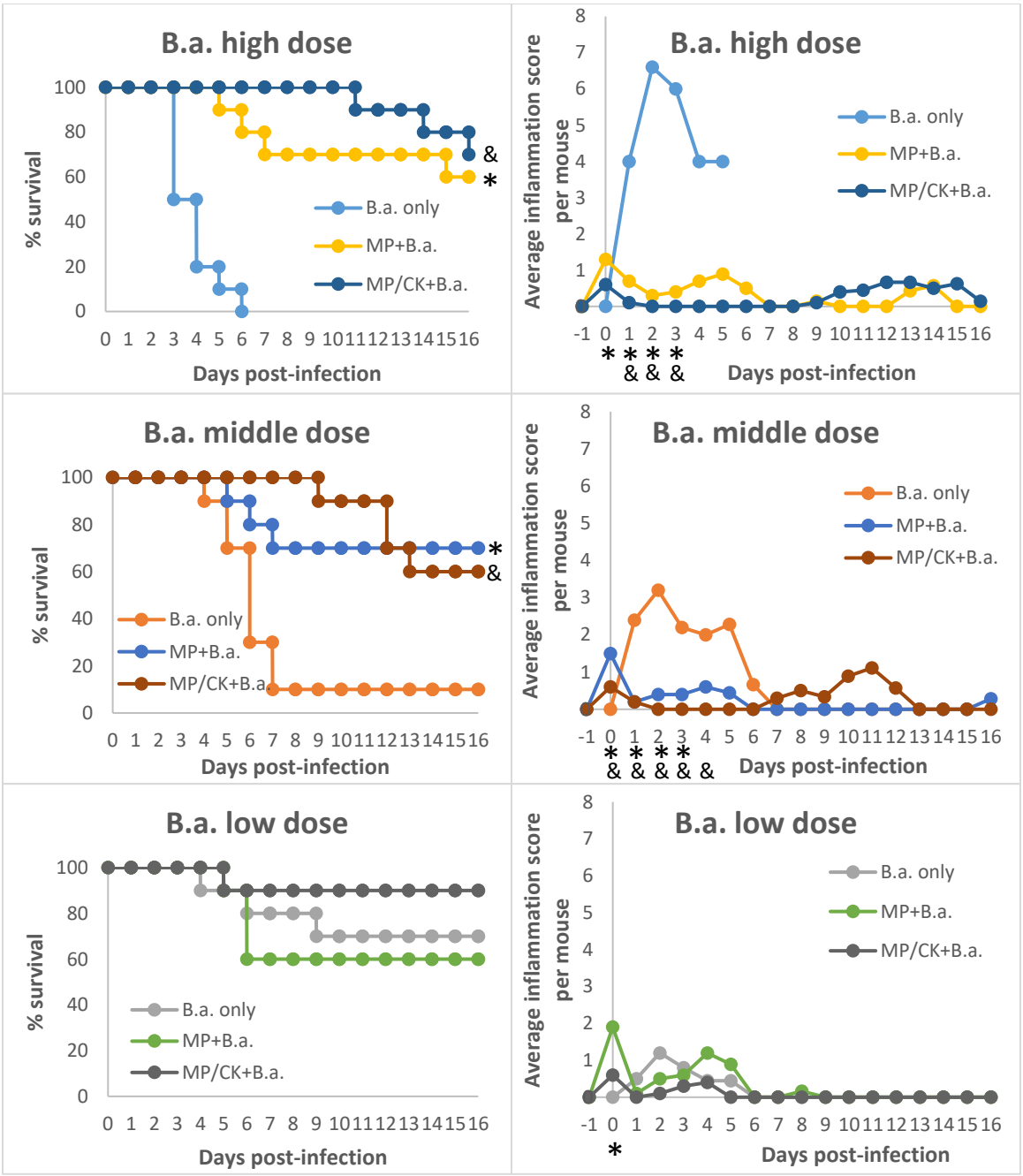

Figure 13. Both MPs and CK-MPs contribute to protection against *B. anthracis* spore challenge.
Animals (n=10/group) were challenged with spores with or without a 20-h pre-treatment injection of MPs or CK-MPs. Spores were administered in a 50 µl volume per FP containing $2.9x10^6$ spores/ml (high dose; 7 LD_{50}s), $9.7x10^5$ spores/ml (middle dose; 2 LD_{50}s), or $3.2x10^5$ spores/ml (low dose; 0.7 LD_{50}s). * and & indicate statistical difference of the MPs or CK-MPs from the control (α=0.05), respectively. Statistical significance of survival (left panels) was determined by the Log Rank Test, and for inflammation (right panels) was determined by the Mann-Whitney U Test.

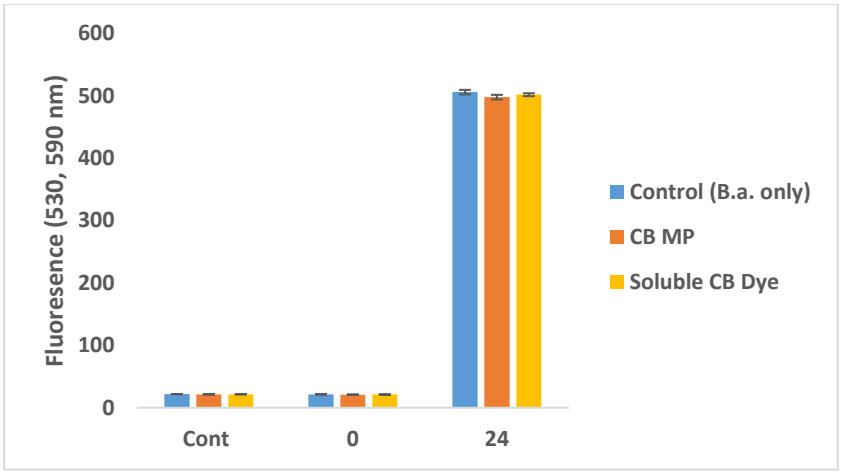

Figure 14. CB MPs and soluble CB dye are not directly toxic to *B. anthracis* spores nor vegetative bacteria. *B. anthracis* spores (800 spores/ml) were incubated with 5% pellet volume of CB MPs or the comparable concentration of soluble CB dye diluted in culture medium. After incubation for up to 24 h, the incubation medium was removed and replaced with Alamar Blue diluted in CSFM and incubated for 1 h. Bacteria and MPs were then removed *via* centrifugation and the fluorescence of the supernatant was measured with excitation at 530 nm and emission at 590 nm. Error bars indicate 95% confidence intervals.

7 p.i. when pre-treated with empty MPs. Comparatively, animals pre-treated with CK-MPs did not reach this level until day 16 p.i.

MPs are not directly toxic to *B. anthracis* spores nor vegetative bacteria

Several hypotheses were considered to explain the effects of empty CB MPs on the outcome of anthrax in our experiments. It was reported that nanoparticles can interact with and penetrate bacterial cells with unique bacteriostatic and bactericidal mechanisms[65]. To test for the potential sporicidal, bactericidal, or bacteriostatic effect of CB MPs, the MPs were incubated with spores in static cultures at 5% CO_2 and 37°C, mimicking the conditions of spore germination and growth within the infected tissues *in vivo*. The impact of MPs on the number of grown bacteria was determined based on the bacterial metabolic activity using Alamar Blue. In control cultures, the spores were incubated in the absence of MPs. As with the assays for cytotoxicity against Raw 264.7

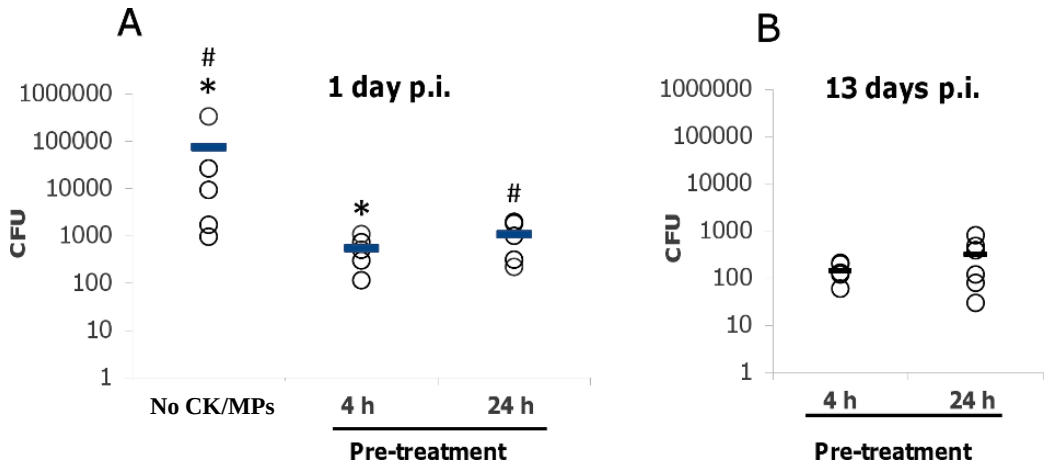

Figure 15. Bacterial load in LNs of spore-challenged mice pre-treated with CK-MPs and control mice at day 1 (A) and day 13 (B).
Animals were injected with $4x10^6$ spores in 20 µl PBS subcutaneously into each hind FP. Bars indicate arithmetic means in each group. Mann-Whitney U-test, *p = 0.02, # = 0.14, *n* = 4-6 per group.

cells, soluble CB dye at a concentration comparable to what is contained within the MPs was included. No effect of the MPs nor the dye on bacterial growth was found after the 24-h incubation indicating that they are neither bactericidal nor bacteriostatic (Figure 14).

The activity of CK-MPs correlates with reduced bacterial burden and influx of neutrophils to the sites of infection and regional LNs

To determine if the protective effect of CK-MPs was correlated with reduced bacterial burden, FPs and popliteal LNs were collected from the surviving mice in these experiments. Both FPs and one popliteal LN from each mouse were taken for histology, while the other popliteal LN was used for estimating bacterial burden. Tissues were homogenized, re-suspended in PBS, and plated on Luria Broth agar plates. The number of colony-forming units (CFU) in pre-treated mice was significantly reduced by nearly 100-fold ($p = 0.02$) relative to the control Group 1 day p.i and remained low until the end

of the two-week period, but the animals were not able to completely clear the infection (Figure 15). Additionally, the duration of pre-treatment (4 h *vs.* 24 h) did not significantly influence the reduction of bacterial burden ($p = 0.14$).

The FP sections were then immunohistochemically analyzed using an antibody recognizing Ly-6G, a surface marker of neutrophils. The antibacterial effect was correlated with an influx of neutrophils to the site of infection and MP injection (Figure 16). Immunostaining of the tissue sections using immunized serum from animals recognizing vegetative *B. anthracis* was also used to further confirm the results described above and to visualize bacterial distribution within the tissue. As expected, mice which did not receive pre-treatment with CK-MPs prior to spore challenge showed intense FP staining 24 h p.i., whereas the bacterial burden was greatly reduced in the pre-treated animals (Figures 17, 18). The FPs of animals which did not receive CK-MP pre-treatment displayed high levels of extracellular bacterial chains and intracellular bacterial antigen (Figure 18A; top panels). In contrast, the positive staining for bacterial antigen in the pre-treated mice was only seen within the cytoplasmic content of phagocytic cells (Figure 18B; top panels).

Consecutive FP tissue slices from the infected animals were further analyzed through staining with antibodies recognizing Ly-6G and CD11b to identify neutrophils and monocytes/macrophages, respectively (Figure 18). These results showed that increased bacterial uptake and elimination of vegetative bacterial chains were correlated with increased phagocytic cell migration in the pre-treated mice. The bacterial-specific

intracellular staining in Figure 18B overlapped with a large area which stained strongly positive for neutrophils and less intensely for macrophages.

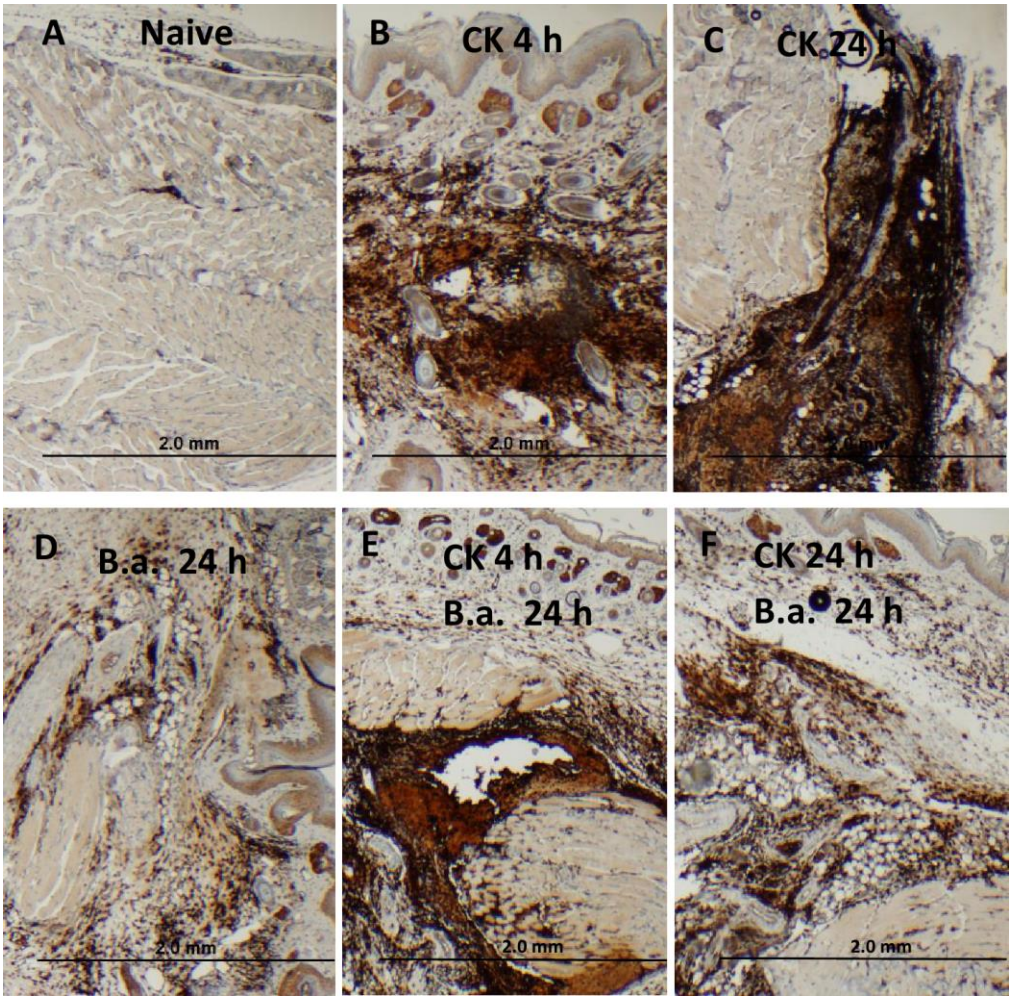

Figure 16. Administration of CK-MPs and spore challenge induce migration of neutrophils to the inoculation site (FPs).
Naïve mice (A) were injected into hind FPs with CK-MPs for 4 h (B) and 24 h (C) and then challenged with *B. anthracis* spores ($0.4x10^6$ per hind footpad) (D-F, correspondingly). At 24 h p.i., mice were euthanized, and the soft tissue from the FPs was removed for the preparation of slides. The presence of neutrophil marker Ly-6G was revealed immunohistochemically (as a brown color of diaminobenzidine stain) using primary antibodies against Ly-6G.

During infection, many of the spores become phagocytosed and are carried to the regional LNs where they proliferate and cause extensive pathological changes[63,66]. Immunohistochemical staining revealed that treatment with CK-MPs drastically changed the pattern of neutrophil staining within the LN (Figure 19). Naïve mice demonstrated occasional high-punctate staining of circulating Ly-6G$^+$ neutrophils (Figure 19A, red arrows). CK-MP administration greatly increased the numbers of Ly-6G$^+$ cells observed, but these cells stained with less intensity (red arrowheads). The lighter staining cells expressing lower levels of Ly-6G represent immature neutrophils which appear associated with HEVs and therefore likely arrived at the LN through the blood.

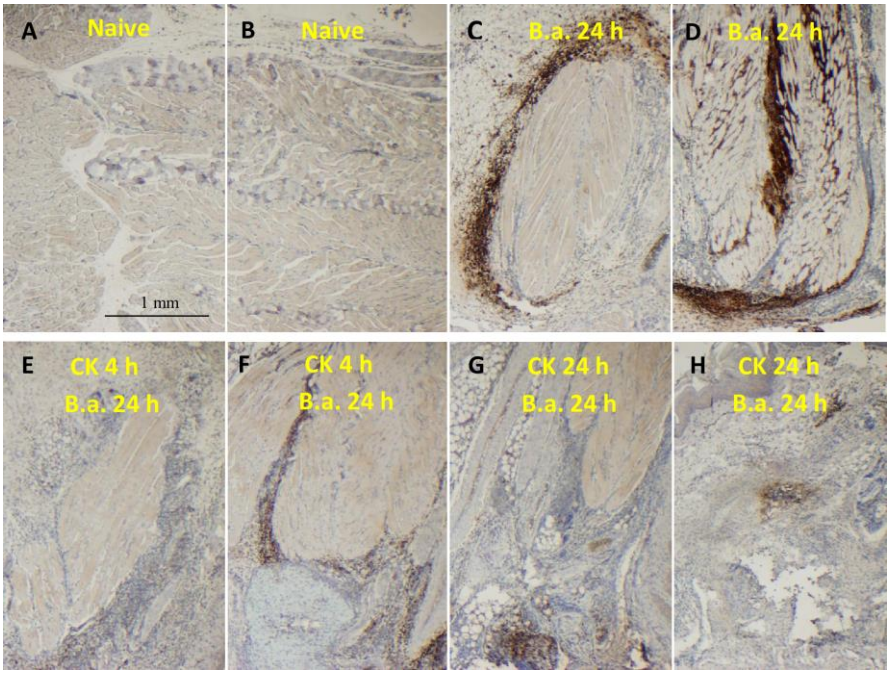

Figure 17. Administration of CK-MPs results in the reduction of bacterial burden in spore-challenged FPs. Mice were challenged with *B. anthracis* spores ($4x10^6$ spores in 20 µl PBS per hind FP) without pre-treatment (C, D) or after pre-treatment with CK-MPs for 4 h (E, F) or 24 h (G, H). At 24 h p.i. the mice were euthanized and FPs immunohistochemically stained brown using α-*B. anthracis* serum. Two representative fields of view are shown for each condition.

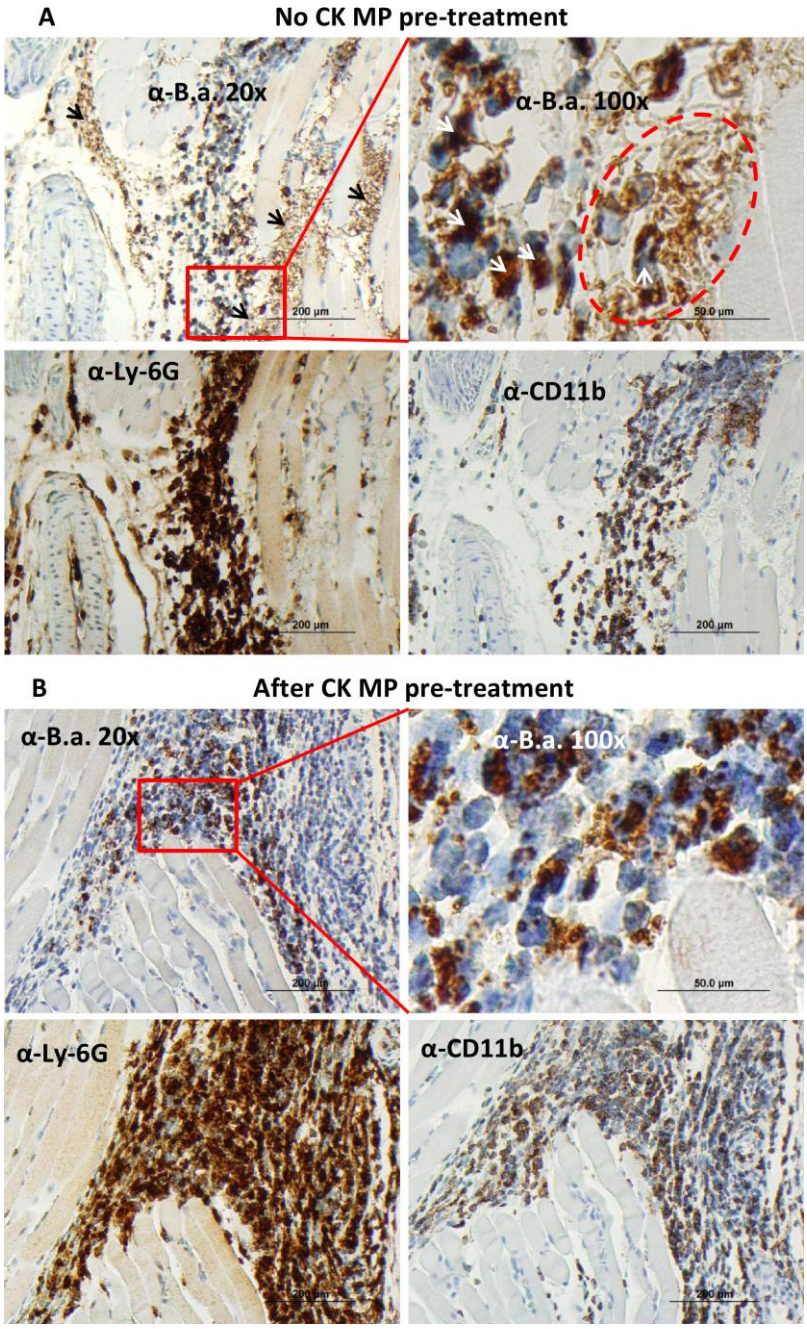

Figure 18. Administration of CK-MPs results in the phagocytic elimination of bacterial burden in spore-challenged FPs.

The presence and distribution of *B. anthracis* spores 24 h p.i. without (A) and with (B) pre-treatment with CK-MPs. $4x10^6$ spores delivered in a 20 µl volume of PBS were injected into each hind FP. Extracellular bacterial chains and intracellular bacterial antigen (brown stain indicated by the black and white arrows, respectively) are present in the top panels of (A), while only intracellular bacterial antigen is present in (B). Red square in the left panel identifies a bacterial swarm (A) which is shown at higher magnification in the right panel next to phagocytes which stained positive for *B. anthracis*-specific antigens. Consecutive slices of tissue stained with α-Ly-6G and α-CD11b (bottom panels, (A) and (B)) demonstrate infiltration of phagocytes to the site of infection.

There were few high-intensity Ly-6G$^+$ cells present 24 h p.i. in the LNs of mice challenged with the high spore dose (4x10^6 spores/ 20 µl; Figure 19B, panel 1). Germinating spores within the LNs induce immunosuppression through their disruption of immune cell function and recruitment[27,33–36]. It was therefore logical that the low spore dose (0.4x10^6 spores/ 20 µl) was less immunosuppressive than the higher dose (4x10^6 spores/ 20 µl), allowing more immune cells to successfully migrate into the LN (Figure 19B, panel 3). The immunosuppression induced at each challenge dose was overcome by the CK-MP pre-treatment, which led to the accumulation of neutrophils in the subcapsular space (Figure 19B, panels 2 and 4).

The evidence of successful early neutrophil recruitment suggests that this contributed to the improved survival of the spore-challenged mice. Consecutive tissue slices from the LNs of the mice surviving at day 13 p.i. from the experiment comparing pre-treatment duration were immunohistochemically stained for *B. anthracis* antigen and Ly-6G$^+$ cells (Figure 20). The overlapping staining for *B. anthracis* antigen and Ly-6G at the end of the two-week period further supports that the early mobilization of neutrophils to the site of bacterial accumulation in the LN was critical for survival. The Ly-6G$^+$ staining is intensely localized within the LN germinal centers (Figure 20, top panels) which are critical sites for connecting the innate and humoral immune responses[67]. The distribution of *B. anthracis* antigen within the germinal centers (Figure 20, bottom panels) appears only intracellularly, suggesting that it is being utilized for antigen presentation to B cells. Other than enlargement relative to those of naïve mice, the LNs of the MP-treated, spore-challenged mice appeared clinically healthy and normal.

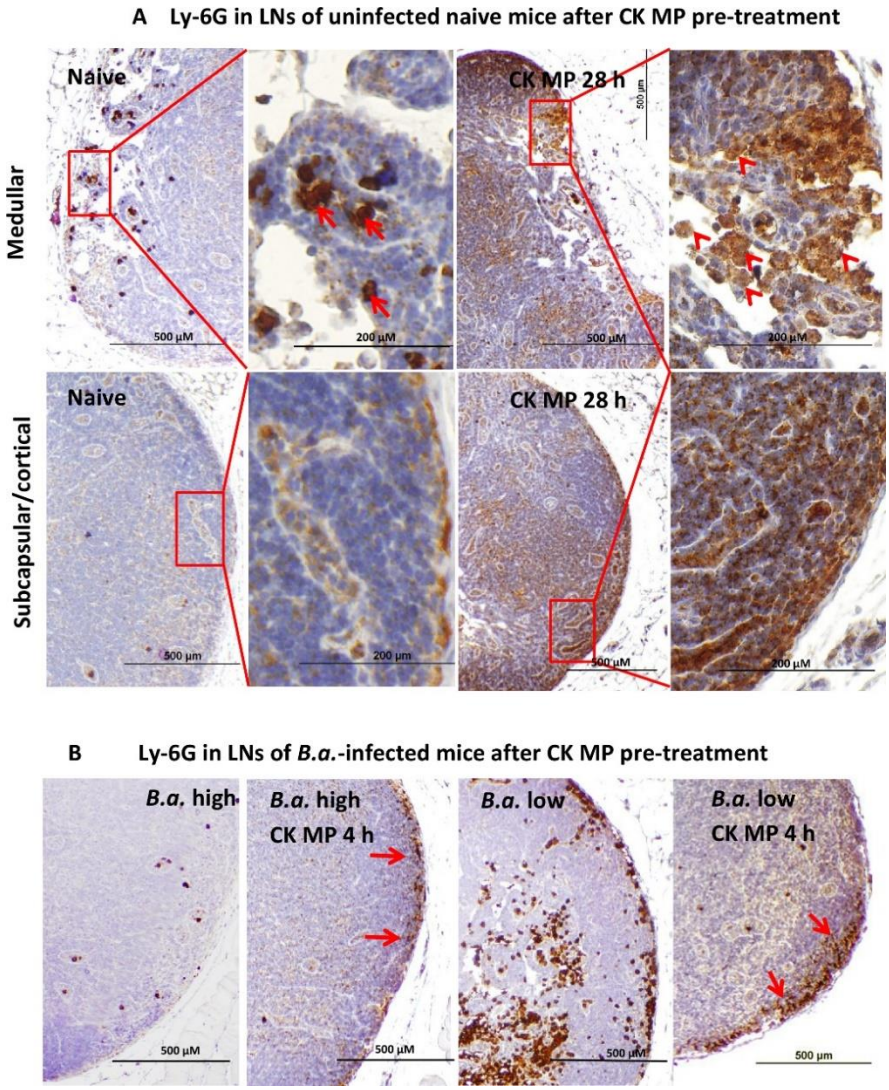

Figure 19. Administration of CK-MPs results in the increased appearance and altered distribution of the neutrophil-specific antigen Ly-6G in the popliteal LNs of naïve and *B. anthracis* infected mice.
(A) Mice were injected into FPs with CK-MPs for 28 h and the presence of Ly-6G$^+$ cells was revealed immunohistochemically (brown color) using a primary antibody against Ly-6G. The magnified squared regions in the right panels show the cells stained with high and low intensities (shown by arrows and arrowheads, respectively). (B) Mice pre-treated with CK-MPs for 4 h and then challenged with *B. anthracis* spores (low, $0.4x10^6$ spores or high, $4x10^6$ spores in 20 µl of PBS) for 24 h. The neutrophils were stained as in (A).

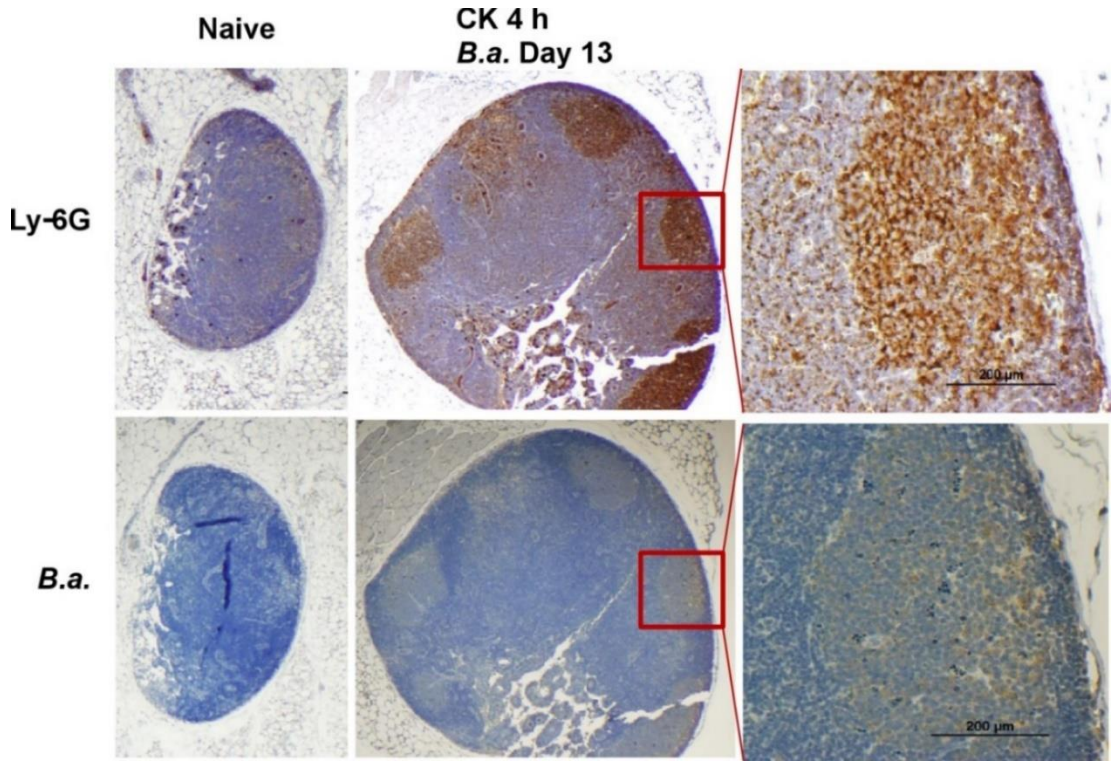

Figure 20. LNs of surviving mice demonstrate size enlargement and the appearance of follicular zones which stain positive for Ly-6G and *B. anthracis* antigens.
Mice were injected into hind footpads with CK-loaded MPs for 4 h and challenged with *B. anthracis* spores ($2.6x10^6$ per hind footpad per 50 µl dose). Naïve mice were left untreated and unchallenged. After 13 days, mice were euthanized, LNs removed and used for the preparation of slides. The presence of neutrophil marker Ly-6G and *B. anthracis* antigens were revealed immunohistochemically (as brown color of diaminobenzidine stain) using the consecutive slices of tissue and primary antibodies against Ly-6G and immune serum against *B. anthracis*, correspondingly. Right panels magnify areas marked in the middle panels with red boxes.

MPs stimulate Raw 264.7 macrophages to release immune response mediators

For analysis of MP immune-stimulating potency, Raw 264.7 macrophages were exposed to MPs or control samples which included serum-free DMEM/F12, LPS from *E. coli*, and the CB dye (preliminarily hydrolyzed as described above). Supernatants were collected and analyzed using the Bio-Rad Bio-Plex Pro™ Mouse Cytokine 23-plex Assay for simultaneous determination of Eotaxin, G-CSF, GM-CSF, IFN-γ, IL-1α, IL-1β, IL-2,

IL-3, IL-4, IL-5, IL-6, IL-9, IL-10, IL-12 p40, IL-12 p70, IL-13, IL-17A, KC, MCP-1, MIP-1α, MIP-1β, RANTES, and TNF-α.

Four cytokines (G-CSF, MCP-1, MIP-1α and TNF-α) were found to be strongly up-regulated in the supernatants of MP-treated cells. The fluorescent signals of these cytokines were detectable as early as 4 h and continued to increase in samples collected at 24 h (Table 2). The concentrations of IL-1α, IL-6, and KC calculated by the Bio-Plex analysis suggested upregulation of their expression, although these values were not statistically significant near the lower limit of detection (not shown). To confirm the Bio-Plex results, quantitative ELISAs were run for the identified CKs (MIP-1α, MCP-1, TNF-α, and KC) (Table 3). Robust responses were detected for MCP-1 and TNF-α. The release of MIP-1α was reliably increased as well, but was associated with a high level of background from unstimulated cells in control medium. KC demonstrated a low-level response to MPs, in agreement with previous reports on exposure of Raw 264.7 cell to a particulate matter[68].

To address the issue of the CB dye within the MPs influencing the magnitude and spectrum of cytokine stimulation, we examined the effect of soluble hydrolyzed CB dye. The dye was diluted to the concentration of allylamine within the MPs. The Bio-Plex assay detected no significant influence of the dye at 4 h for any of the cytokines. Longer incubation (24 h) strongly influenced expression of G-CSF; however, the level of stimulation was much below that of MPs. Higher concentrations (up to 10x) of dye significantly enhanced the levels of IL-12(p40), MIP-1α, MIP-1β, and TNF-α detected at

Table 2. Fluorescence results from the Bio-Plex Pro™ 23-plex Assay of cytokine production by Raw 264.7 cells.

	CB MPs (10% pellet)				CB dye	
	4 h		24 h		4 h	24 h
Cytokine	**Control medium**	**CB MPs**	**Control medium**	**CB MPs**	**1x Concentration**	**1x concentration**
G-CSF	29	190 86 [&]	138	16,221 3,420 [&]	33	582
MCP-1	469	262 2,576 [&]	528	19,473 21,298 [&]	325	816
MIP-1α	12,205 *	5,019 * 13,414 * [&]	15,685 * ULOQ	16,694 * ULOQ 18,586 * [&] ULOQ	12,763 *	15,785 * ULOQ
TNF-α	27	4,553 1,870 [&]	25	2,709 * 8,318 [&]	23	67
KC	43	32 49 [&]	63	72 74 [&]	46	67

Cells in serum-free DMEM/F12 were exposed to CB MPs (at 10% or 2.5% bead volume) or hydrolyzed CB dye (at concentration equal to that in MPs) for 4 h or 24 h. Only cytokines with fluorescence signals which were substantially increased in at least one of the MP- or dye-treated samples relative to the control are shown. KC as an exception was included here as it was shown by ELISA and immunohistochemical staining to be increased in response to MP treatment. All values represent the average fluorescence signal after background subtraction of undiluted samples measured in triplicate. * indicates average fluorescence of samples which had been diluted 10-fold in serum-free medium measured in duplicate. [&] indicates the response to MPs at 2.5% bead volume. MIP-1α values exceeding the upper limit of quantification (ULOQ) of fluorescence intensity are shown. MIP-1α ULOQ is approximately 13,710 RFU.

Table 3. Results of ELISAs of chemokine production by Raw 264.7 cells.

	4 h		24 h	
Cytokine	**Control medium**	**CB MPs**	**Control medium**	**CB MPs**
MCP-1	69±7	10%: 111±53 5%: 77±43 2.5%: 58±13	221±22	4,040±214 1,648±125 922±26
MIP-1α	ND	ND	10,923±434	17,873±334 10,563±214 11,938±122
TNF-α	46±6	1,445±98 1,568±124 1,976±61	59±5	9,880±383 10,151±163 8,802±532
KC	ND	ND	<16 Below LLOQ	10%: 76±24 3.3%: 76±28 1%: 26±11

ELISAs were performed using supernatants of cells exposed to CB MPs or hydrolyzed CB dye to more precisely confirm the concentrations of chemokines which had increased signal relative to untreated cells according to the Bio-Plex Pro™ 23-plex Assay. The concentrations in pg/ml ± CI (α= 0.05) shown here represent values calculated after accounting for sample dilution. The three values per cell in the CB MP columns represent MCP-1, MIP-1α, and TNF-α responses to 10%, 5%, and 2.5% bead volumes, notated from top to bottom. For KC, the three values represent responses to 10%, 3.3% and 1% bead volumes. ND = analysis not done. LLOQ = concentration below the lower limit of quantification

24 h in a dose-dependent manner (not shown). However, these results can only be used to demonstrate the potency of the free dye because such high concentrations (10-fold greater than the concentration of allylamine groups) cannot be coupled to the MPs. Overall, the above data suggest a low stimulating activity of the coupled dye, considering that only a fraction of its concentration within the MPs is expected to be accessible to the cells.

An additional experiment was conducted with allylamine MPs not coupled with the CB dye. As determined by ELISA, the KC-stimulating activity of the allylamine MPs (178 pg/ml after 24 h; data not shown) was almost 6-fold higher than in the case of CB MPs, implicating factors other than the CB dye in the effect of MPs. It has been previously shown that Raw 264.7 cells do not greatly express KC, even when exposed to significant concentrations of LPS[68]. The slight increase in KC expression observed with this cell type is not predicted to be biologically significant, but suggests that other cell types which are more capable of producing KC may have significantly increased KC production in response to MP exposure. Indeed, immunohistochemical staining of FPs confirmed increased KC expression in response to MPs *in vivo* (data not shown).

As described earlier, the MPs and their loaded CKs each contributed to the protection observed in spore-challenged mice (Figure 13). To support the hypothesis that *in vivo* induction of endogenous CKs played a protective role, FPs from animals treated with MPs were stained for neutrophils using Ly-6G as before. Figure 19 clearly demonstrates that CK-MPs induced migration of Ly-6G$^+$ neutrophils to the LN. Here we stained FPs to see if the increased expression of KC, which is a neutrophil-attracting CK, was associated with the MPs and/or their CK content. Animals were treated with AA

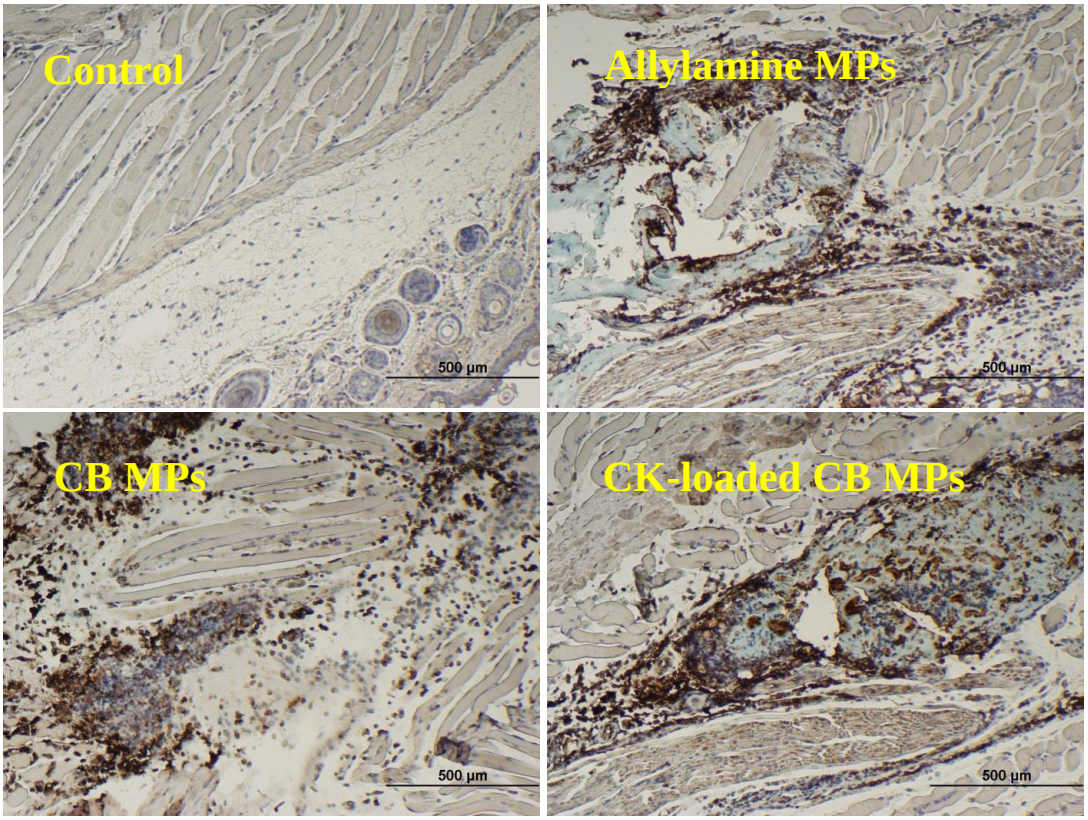

Figure 21. FPs of animals treated with AA MPs demonstrated increased response of Ly-6G+ cells irrespective of the presence of coupled CB dye and/or loaded CKs.
Mice (n=2-3) were treated with AA MPs (10% wet *v/v*) with/without the coupled CB dye with/without loaded CKs (1 µg/ml each of IL-8 and MIP-1α) for 24 h. FPs were immunohistochemically stained with the neutrophil-marker Ly-6G, visualized as the dark brown stain.

MPs coupled with CB dye with/without bound CK or with AA MPs which were not coupled with dye and sacrificed after 24 h. In all groups, the number of Ly-6G$^+$ cells in the FPs increased (Figure 21).

MPs stimulate migration of Langerhans cells *via* ERK1/2 activation

As mentioned, the release of inflammatory CKs and TNF-α by RAW 264.7 cells in response to MPs suggested that MPs could stimulate the immune cell traffic *in vivo*. Both MCP-1 and MIP-1α can be produced by different cell types, including epithelia and

endothelial cells, macrophages, fibroblasts, etc. These CKs are known to induce chemotaxis of mononuclear phagocytes and lymphocytes, while neutrophils can respond to KC as well as MIP-1α both *in vivo* and *in vitro*[69,70]. It was reported that neutrophil migration in immunized mice depends on the release of MIP-1α, which acts *via* the sequential release of TNF-α and Leukotriene B4[71]. CC chemokines such as MCP-1 and MIP-1α are critical for leukocyte recruitment during Th1-type cell-mediated immunity to pulmonary *C. neoformans* infection[72]. Neutralization of TNF-α in mice decreases the levels of both MCP-1 and MIP-1α[73] and strongly ablates the migration of leukocytes (macrophages, neutrophils, and $CD4^+$ T cells) demonstrating that TNF-α is a proximal mediator for chemokine induction.

As described above, immunohistochemical staining of FP slices for Ly-6G showed that injection of MPs with the coupled CB dye (CB MPs) or uncoupled allylamine MPs induced a strong migration of neutrophils (Figure 21). A similar picture was found in the case of MPs loaded with CKs (IL-8 and MIP-1α). This prompted us to suggest that the endogenous neutrophil chemoattractants induced by MPs and the exogenous CKs loaded onto MPs might be working on the same or closely related (overlapping) pathways. One of the plausible mechanisms of MIP-1α and MCP-1 upregulation by the subcutaneously injected MPs in our experiments can be the activation of ERK1/2 pathway of Langerhans cells[74]. Langerhans cells are resident antigen-presenting immune cells of the skin and mucosa. Although classically identified as DCs, these myeloid-derived (macrophage) Langerhans cells uptake antigen from peripheral tissues and migrate inward toward the local LN upon activation. The population of skin

cells highly positive for the activated (phosphorylated) form of ERK1/2 was readily detectable in the epidermis of naïve mice as a layer above the stratum spinosum (Figure 22). At 48 h p.i. using CK-MPs, the pERK1/2^{+} cells were found migrated through the stratum spinosum (which is directly above the epidermal basal layer) into a deeper, dermal location. A similar effect took place in the spore-challenged mice after the 4-h pre-treatment with CK-MPs. The migration was accelerated and could be detectable as soon as 24 h following spore challenge, while no migration took place at this time in infected mice without the MP pre-treatment. The infectious process resulted in the depletion of pERK1/2^{+} cells increasing with the challenge dose, and the MP pre-treatment showed a protective effect.

Langerhans cells encountering antigens are known to migrate to regional LNs and display the MHC-class II (MHCII) molecules. Consistent with this, the pERK1/2^{+} cells in the popliteal LNs increased after injection of MPs. Patterns of immunohistochemical LN staining probing consecutive tissue slices with antibodies against pERK1/2 and MHCII closely overlapped (Figure 23). Taken together- the characteristic morphology of the migrating cells in the skin (Figure 22), their positive staining for ERK1/2 and MHCII (Figure 23), their initial epidermal location, as well as the capacity to migrate into dermis and LNs upon exposure to antigens, identified these cells as Langerhans cells.

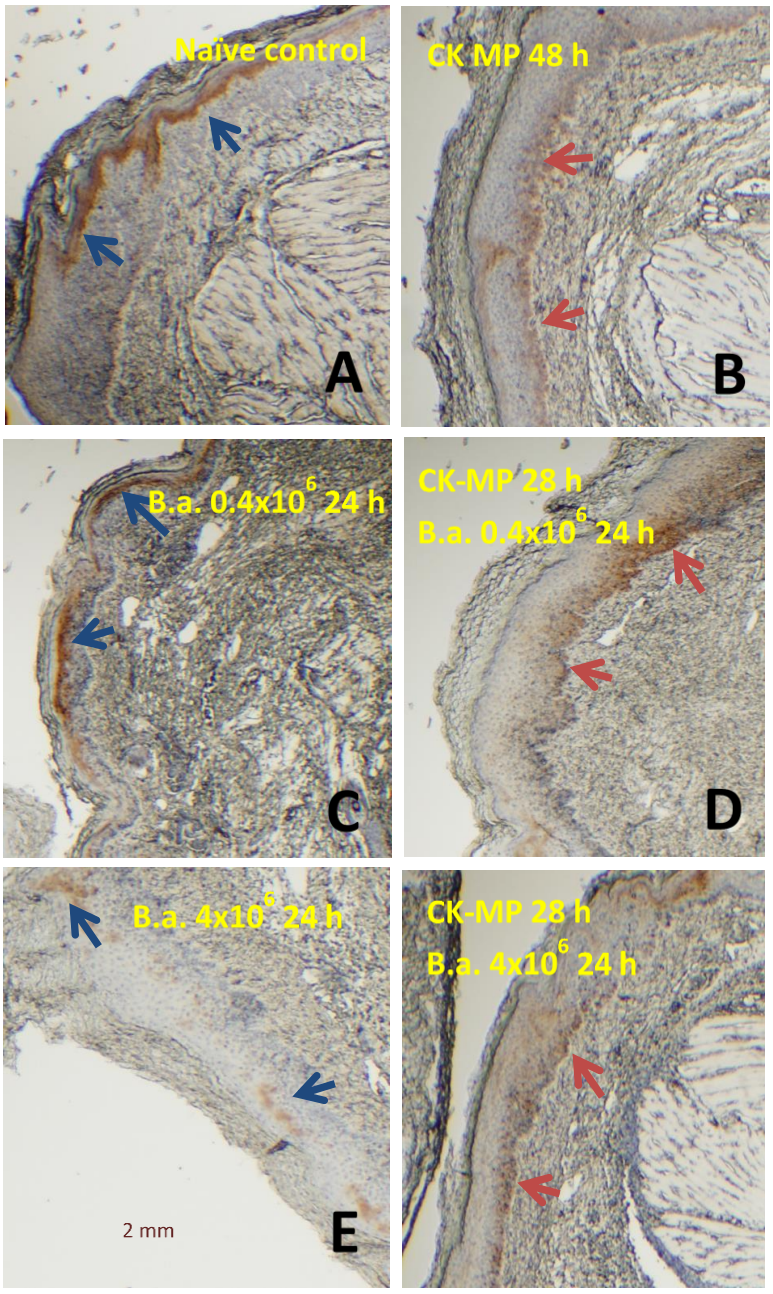

Figure 22. Administration of CK-MPs changes the distribution of pERK1/2$^+$ cells at the site of injection (FPs). pERK1/2$^+$ cells in naïve and spore-challenged animals which did not receive CK-MPs were present as a distinct epidermal layer (left panels). Positively-staining cells in animals treated with CK-MPs were found migrated from their epidermal location to deeper dermal layers. Challenged animals received 50 µl injections of *B. anthracis* spores and/or CB MPs loaded with 1 µg/ml of each MIP-1α and IL-8. Animals receiving CK-MPs were treated for either 4 h or 24 h prior to spore challenge and sacrificed 24 h after infection, notated as 28 h and 48 h, respectively.

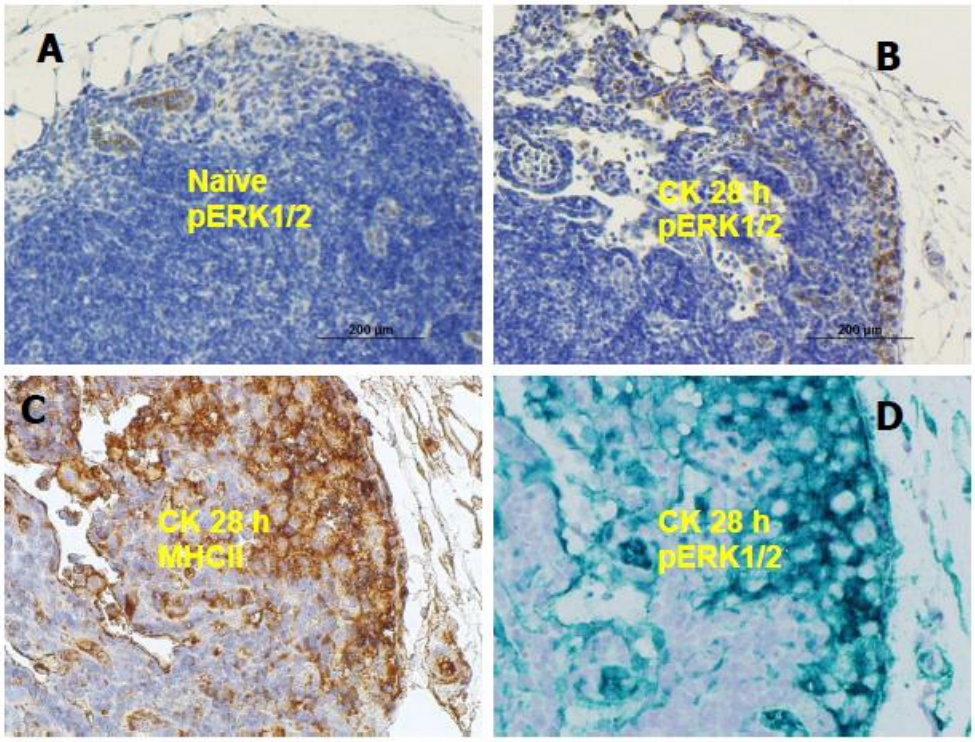

Figure 23. Distribution of pERK1/2^{+} cells and MHCII^{+} cells in the LNs following CK-MP treatment.
(A, B) Medullar region of popliteal LN in naïve mice (A) or after injection of CK-MPs for 28 h (B) under 40x magnification. Immunohistochemical staining with pERK1/2-specific antibody. (C, D) Overlapping patterns of immunohistochemical staining of LNs of mice injected into hind FPs with MPs for 28 h. Primary antibodies against MHC II (C) and pERK1/2 (D). For each pair of images in (C, D), consecutive slides of LN tissue were used and colorimetrically developed with diaminobenzidine (brown color, (C)) or Emerald Green (green color, (D)).

DISCUSSION

For the development of a novel MP-based platform for sustainable immunomodulation, we have demonstrated the feasibility of using MPs for binding and releasing multiple CKs. The incorporation of different capture dyes into functionalized MPs allowed for different rates of CK binding and release, determined by the specific kinetics of each CK-MP pair. Diffusion of small, cationic CKs into MPs coupled with dyes containing anionic sulfate groups and substituted aromatic rings allowed for their retention and stabilization within the MPs. The CK-MP pairs tested demonstrated low micromolar to high nanomolar affinities (Figure 3), similar to other techniques aimed at achieving sustained delivery of a drug or biomolecule for therapeutic purposes[45,46]. This allows for the sustained release of CK from MPs for more than 20 h *in vivo* (Figure 4, Table 1).

Although the best conditions identified for loading CK into MPs utilized PBS diluted 1:3 with water with overnight incubation at 4°C (Figure 2), most experiments were carried out with undiluted PBS as the CK-MP suspension would be injected into animals. Binding in full-strength PBS mimicked the physical characteristics of blood and lymph. Loading CK into MPs in mild physiological conditions eliminates complications associated with many previous MP-based approaches. Our *in vitro* results showed that injection of CK-MPs into animals leads to the rapid release of a loosely-bound fraction of

CK followed by sustained dissociation of the remaining CK into solution, in accordance with patterns of first-order kinetics.

Physical characteristics of MPs and experimental conditions that were anticipated to be problematic did not appear to have any adverse influence on our results. In contrast to previous studies suggesting the collapse of thermoresponsive polymers at higher temperatures leading to entrapment of their cargo[45], our MPs released CK more rapidly at 37°C relative to room temperature (Figure 4A-B). Additionally, the presence of large proteins like albumin in the solutions used for CK binding and release did not significantly interfere with either of these steps (Figure 4C). The pore size of our MPs effectively excluded proteins larger than 20 kD. This importantly allows for binding even in solutions which contain BSA as an additive for preventing the aggregation or inactivation of CKs and other proteins.

We have proposed using CK-MPs for controllably and sustainably delivering CK for directed immune modulation. As a preliminary assessment of safety, we confirmed that our MPs are not directly toxic to Raw 264.7 macrophages, a cell line commonly used for analyzing MP cytotoxicity (Figure 6)[55–57]. Subcutaneous injection of MP suspensions into the hind FPs of mice resulted in their localization to the regional popliteal and inguinal LNs. The MPs become distributed primarily in the subcutaneous and medullary regions of the LNs, likely reflecting their modes of arrival to these sites (Figure 7). Several characteristics of MPs have been shown to influence their diffusion and/or other transport modes through the lymphatics. Large MPs (>500 nm) have decreased ability to enter the lymphatics, so it is expected that passive diffusion through the lymphatics may

only partially explain the appearance and distribution of our MPs. It is more likely that tissue-resident macrophages or DCs in the FP gradually phagocytosed the MPs (which are comparable in size to bacterial cells) and carried them to the LN, which would explain their high abundance in the medullary region.

Empty RB MPs (without CK) induced low levels of neutrophils responding shortly after injection but which dissipated within 24 h (Figures 8, 10). In contrast, the MPs loaded with IL-8 (CXCL8) and MIP-1α (CCL3) induced sustained neutrophil migration (Figures 9, 10). A combination of CXC- and CC-class CKs was chosen as they were expected to display a synergistic effect through their interactions with different families of receptors. Human IL-8 is analogous to mouse MIP-2 and KC, which are chemoattractant for neutrophils. It has well-established cross-species reactivity in mice for activation of the CXCR1 and CXCR2 receptors[75–78]. Murine MIP-1α is also chemoattractant for neutrophils and is a general activator of granulocytes[79]. It enhances the inflammatory response by inducing the synthesis and release of pro-inflammatory CKs including IL-1, IL-6, and TNF-α from fibroblasts and macrophages[80].

The induction of neutrophil migration in response to CK-MPs confirmed *in vivo* the results from the *in vitro* transwell migration assays (Figure 5). Not only did the MPs protect the loaded CK against aggregation and proteolytic degradation, but they were also successfully able to retain CK functionality *in vivo*. The release of functional CK from MPs induced significant neutrophil migration into the subcapsular and medullary regions of the LN, where the MPs had accumulated. Neutrophil accumulation in the subcapsular

region is indicative of arrival *via* the afferent lymphatics, whereas those in the medullary regions likely arrived through extravasation from the blood *via* HEVs[62,81].

The half-lives calculated for IL-8 and MIP-2 *in vitro* and the estimate that different MP-CK pairs would release biologically significant amounts of CK for more than 20 h were also supported. Mice injected with MPs containing IL-8 and MIP-1α demonstrated increasing levels of neutrophils in the LNs over a 24-h period in a dose-dependent manner. In contrast, mice injected with soluble CK demonstrated the highest neutrophil response at 4 h which had decreased by 24 h. Thus, the MPs are a critical vehicle for maintaining sustained delivery of functional CK for the direction of immune cell migration to and within the LN.

Induction of sustained immune migration is a desirable therapeutic technique which, if sufficient, may avoid treatments involving harsh chemotherapies. Immunosuppression is an important mechanism by which many disease agents avoid elimination so we next tested the ability of the CK-MPs to overcome immunosuppression induced by *B. anthracis*. We pursued neutrophil-attracting CKs for the superior elimination capabilities by neutrophils of many infectious agents. Neutrophils are one of the first responding immune cell types and can eliminate pathogens through the release of lytic enzymes, production of reactive oxygen intermediates, and neutrophil extracellular traps[82–84]. Neutrophils from humans and mice have been shown to kill *B. anthracis* spores and vegetative cells *in vitro*[85–87]. However, *B. anthracis* disrupts CK signaling and actin-based neutrophil migration *in vivo*, preventing these cells from exerting their bactericidal effects[36].

Our results repeatedly showed that timely stimulation of neutrophils (marked by Ly-6G) and monocytes/macrophages (marked by CD11b) by CK-MPs provided significant protection in animals challenged with *B. anthracis* (Figures 11, 16, 18, 19). Neutrophil migration was induced in both the LNs and FPs, where portions of the MPs accumulated. These are also the sites of bacterial accumulation and proliferation. Prophylactic administration of CK-MPs effectively reduced the bacterial burden through successful phagocytic elimination. Bacterial titers in the LNs were reduced in pre-treated animals and remained low through the duration of the two-week survival analysis (Figure 15). Further evidence of this is that the bacterial antigen observed in the pre-treated animals was primarily located intracellularly in association with Ly-6G^{+} cells, likely in the form of digested bacterial antigen used for presentation to cells of the adaptive immunity (Figure 18).

Improved survival in the pre-treated animals was correlated with an initial reduction of FP inflammation. This effect was most prominently observed in the group which only received one pre-treatment injection of CK-MPs (Group 4, Figure 11). Development of a second phase of FP inflammation later during the infectious process coincided with the end of CK release from the MPs (occurring after five half-lives) and likely the induction of an adaptive immune response. Alternatively, the second phase of inflammation which was correlated with a delayed onset of mortality in CK-MP pre-treated mice may represent the delayed germination of dormant spores. Comparatively, all animals in the spore-challenged control group rapidly developed extensive FP inflammation which correlated with rapid onset of mortality. Animals which received two

post-infection injections of CK-MPs without pre-treatment (Group 6) were unexpectedly statistically similar to the control group for both survival and inflammation. This clearly supports that early induction of an immune response is critical for survival in spore-challenged animals. Rapid dissemination of spores through the lymphatics to distant locations, including the spleen, has previously been observed within as little as 3 h[88]. Germination of the spores in the LNs and more distant sites followed by production of immunosuppressive virulence factors allows for unimpeded bacterial proliferation, tipping the odds of survival in favor of the bacterium.

An additional survival analysis experiment was conducted to determine the importance of the duration of CK-MP pre-treatment (data not shown). Animals were prophylactically treated with CK-MPs for 4 h or 24 h prior to spore challenge. Prophylactic administration of CK-MPs at either time statistically improved protection, resulting in an average between all three pre-treated groups of 53% survival for up to two weeks. In comparison, death of all mice in the control groups occurred within either four or six days p.i. In both experiments, the bi-phasic development of inflammation occurred. The success of the brief 4-h pre-treatment and the predominant prevalence of Ly-6G$^+$ cells compared to CD11b$^+$ ones (Figure 18) likely suggests that the majority of the cells recruited by CK-MPs were resting neutrophils (CD11b$^-$Ly-6G$^+$) from nearby circulation, which can be activated by IL-8 to become CD11b$^+$[89,90]. The quick, sustained mobilization of these circulating cells by CK-MPs greatly contributed to protection.

The survival analyses first described (Figure 11 and from data not shown) involved injection of spore inocula which were at least 100-fold greater than the LD_{50} for

this model of injection. Spore challenge using lower inocula doses (from 0.7x- to 7x-LD_{50}s) allowed us to discern the important individual contributions by the MPs and their loaded CKs toward survival outcome (Figure 13). Multiple hypotheses were investigated to determine what role the MPs alone played in improving survival in spore-challenged animals. Previous studies have shown that nanoparticles can be bacteriostatic or bactericidal through interaction with and penetration of bacterial cells[65]. In our study, neither the CB MPs nor the coupled CB dye were inherently toxic toward the spores nor the vegetative bacteria (Figure 14). Instead, we found that the MPs have immune-stimulatory properties to induce endogenous production of multiple pro-inflammatory CKs by the host. *In vitro* analyses using Raw 264.7 macrophages demonstrated increased expression of G-CSF, TNF-α, MCP-1, and MIP-1α in response to MPs (Tables 2, 3). IL-1α, IL-6, and KC were suggested by the Bio-Plex results to be elevated in response to MP exposure, but were not statistically reliable as the fluorescence was near the machine's lower limit of detection. KC is only minimally expressed by Raw 264.7 cells even in response to significant concentrations of LPS[68]. The slight increase in KC production observed in this cell type would thus not be biologically relevant on an organismal level. However, immunohistochemical staining of FPs confirmed that KC expression is increased in response to MP treatment (data not shown). Possible upregulation of IL-1α and IL-6 in response to empty MPs would act in redundancy with delivered MIP-1α stimulation of these CKs[80], further enhancing immune response. The absence of IL-1β response indicated that neither the MP scaffold nor the coupled dye activated the inflammasome in RAW 264.7 cells, in contrast with what was observed in the case of

several nanomaterials[91,92], including the MPs loaded with LPS[93,94]. It also showed that the LPS commonly contaminating the MP preparations was unlikely to contribute to our results.

Further support in favor of the MPs playing an important protective role comes from *in vitro* studies utilizing one batch of MPs which was portioned for coupling with the CB dye for different amounts of time. Large CB-coupled agarose beads have been previously shown to induce inflammation with predominant neutrophil and macrophage activity upon injection[95]. For our CB MPs, it appears that the incubation time for coupling with the dye influences the amount of dye within the MPs. This is evidenced by MPs coupled with CB dye for 48-h binding more CK from solution compared to those coupled for only 24-h (data not shown). Incomplete dye coupling suggests that the amines from more of the allylamine functional groups remain exposed. Exposed primary amines *in vivo* serve as immunogens and inducers of interferon production[96]. Interferons are important pro-inflammatory cytokines which activate innate immune cells and promote antigen presentation by increasing their MHC expression. Exposed primary amines have also been investigated as functional groups to enhance the phagocytosis of MPs and their subsequent clearance from circulation[97]. Although our CK-MPs conferred the highest protection against *B. anthracis*, incomplete dye coupling and correspondingly slightly lower levels of bound CK may not necessarily be considered as a negative factor. Factors capable of directly inducing leukocyte migration (the CK released from our MPs) and/or indirectly through induction of endogenous CK expression may each find utility for enhancing immune responses.

Our observations with RAW 264.7 macrophages parallel several reported examples of the responses of macrophages and DCs toward MPs. The activation of innate responses in macrophages by poly(lactide-co-glycolic acid) (PLGA) nanoparticles improves the outcome of infection with *Leishmania braziliensis*. The decreased parasite load *in vitro* is associated with the augmented production of nitric oxide, superoxide, and IL-6. An increased release of TNF-α, MCP-1 and KC also takes place, resulting in macrophage and neutrophil recruitment *in vitro*[92].

DC responses to MPs have also been reported. As with macrophages, MP stimulation can induce DCs to enhance inflammatory CK and cytokine production, as well as co-stimulatory molecules when the MPs are phagocytosed[98]. The 200 nm-sized biodegradable poly(gamma-glutamic acid) MPs are activators of human monocyte-derived DCs producing IL-8, MIP-1α, MIP-1β, and MCP-1. In addition, TNF-α and IL-1β were detected, albeit at a lower level.

Carboxylated polystyrene MPs are shown to modulate DC homeostasis, thereby promoting a persistent enhanced state of immune readiness to a subsequent infectious challenge[99]. Intradermal administration of these MPs induced anti-inflammatory cytokines, CKs and growth factors, increased numbers and proportions of DCs in the draining LNs, and increased the capacity of bone marrow to generate DCs. Consistent with this observation, mice pre-injected with the MPs showed enhanced ability to generate anti-malarial immunity. Neutrophil recruitment in immunized mice was shown to depend on MIP-2 inducing the sequential release of MIP-1α, TNF-α and Leukotriene B4[71,100]. MCP-1 and MIP-1α mediate firm adherence and subsequent transmigration of

neutrophils *via* protein synthesis and secondary generation of leukotrienes and Platelet-Activating Factor, which in turn directly activate neutrophils[101]. The lifespan of the latter can be extended by G-CSF[102]. Taken together, the above features of the MP interaction with the immune system resulting in the release of CKs and recruitment of immune cells represent a likely explanation of our observations on the protective effect of MPs.

Secretion of MIP-1α by neutrophils resulting in DC recruitment in the case of *Leishmania major* is shown to confer protection against intradermal inoculation of the parasite, as markedly decreased DC recruitment is observed in mice depleted of neutrophils or deprived of the capacity to produce MIP-1α[103]. The release of MIP-1α and IL-8 may be secondary to the induction of initial migration of DCs and monocytes as it was shown for acute-phase protein amyloid A produced during infection by hepatocytes, adipose tissue, endothelial cells, and macrophages. These CKs enhance DC migration and promote the recruitment of distant cells (such as neutrophils)[104]. Our data *in vivo* confirm recruitment of neutrophils and migration of epidermal cells with characteristic features of skin Langerhans cells from epidermis to dermis and subsequently to LNs in response to MPs (Figure 22). These effects are expected to be enhanced in the case of CK-loaded MPs delivering exogenous MIP-1α and IL-8, in agreement with the additional protection conferred by these CKs in spore-challenge experiments (Figures 11, 13, and data not shown). The migrating cells displayed activation (phosphorylation) of ERK1/2 indicative of their MAPK-induced maturation through up-regulation of co-stimulatory molecules[74]. The migration of $pERK1/2^{+}$ cells was not detected without MPs. The infection process resulted in the elimination of ERK1/2 activation in control mice, in accordance with the

well-known capacity of anthrax toxins to target macrophages and DCs and downregulate the MAPK signaling[105], while administration of MPs showed a protective effect.

We showed that our MPs are actively trafficked to the regional LNs from the injected FPs. Here we found that the MPs strongly increased pERK1/2 expression by $MHCII^+$ cells, indicating their Langerhans phenotype. The distribution of the $pERK1/2^+MHCII^+$ cells in the subcapsular and medullary regions within the LN (Figure 23) is reminiscent of the fluorescent MPs distribution (Figure 7), providing further evidence that the tissue-resident Langerhans cells as well as circulating $Ly\text{-}6G^+$ neutrophils were responding to MP administration.

Prolonged exposure to the immune-stimulating MPs remains a concern prior to their potential clinical application. Persistent production of inflammatory CKs is associated with numerous pathologies which may occur locally or systemically. In the skin and muscle, this is associated with psoriasis[106], arthritis[107], fibrosis[108], and numerous idiopathic inflammatory myopathies[109]. Chronic inflammation in the brain can contribute to progression of neurodegenerative disorders including Alzheimer's disease, Parkinson's disease, amyotrophic lateral sclerosis, and multiple sclerosis[110,111]. Chronic inflammation spreading beyond a local tissue or organ can result in the systemic cytokine storm[112].

As our MPs induced endogenous pro-inflammatory CK production and persisted in both the LNs and the FPs, it may be suggested that this could result in the development of pathologies associated with sustained inflammation. We did not observe any adverse effects of MP exposure by the end of a two-week exposure, but events occurring after longer exposure times were not measured.

It is well-established that MP physical properties such as size, shape, and surface modifications strongly influence their cellular uptake and tissue distribution *in vivo*[61,113–115]. Modification of MP surface charges frequently involves the addition of carboxyl or amine groups[116]. Recent studies have shown that cationic MPs may induce adverse reactions through alteration of mitochondrial and endoplasmic reticulum function, induction of reactive oxygen species and pro-inflammatory CKs, and cell death[117–119]. Comparatively, anionic MPs have been associated with little to no toxicity[113]. MPs possessing a strong negative charge (with overall charge below -30 mV) have been identified as anti-inflammatory and can further induce antigen-specific immune tolerance when combined with antigen[120–122].

Our MPs were coupled with the anionic CB dye. Based on charge alone, our results of CB-coupled MPs inducing pro-inflammatory CK production (Tables 2, 3) conflict with literature evidence that these MPs should be anti-inflammatory. However, as described earlier, batches of MPs which were incubated for longer times during dye coupling likely bound more dye, as measured by their abilities to bind more CK (data not shown) and thus likely possessed a weaker negative charge due to the presence of uncoupled positively-charged AA amines. The strength of the charge and amount of CB dye coupled into the MPs was not measured. The influence of the CB concentration within our MPs on each the protective effect against *B. anthracis*-challenged animals and on potential toxicity or pathogenicity associated with long-term MP exposure remains to be experimentally tested. For this to proceed as a potential therapeutic option, it will be important to evaluate if making the MPs less immunogenic (through longer times for dye

coupling) would influence their immune-modulating abilities. CK-MPs demonstrated the best protection against anthrax, and it may be likely that loading the MPs with CKs containing higher CB dye levels could promote tolerance by the host to their persistence and protect against the development of chronic inflammation associated pathologies.

CONCLUSION

The issue of disease-induced immunosuppression has gained much attention by modern researchers in the medical field. Disease agents which are capable of escaping the body's immune defenses frequently cannot be sufficiently treated and can have fatal outcomes. Among bacteria, *B. anthracis* is a striking example of such a problematic infection. The ability of this bacterium to suppress the host immune response and reside dormant within the body enables it to withstand elimination by current therapeutic techniques. The mortality rate among those who acquire the bacterium through certain modes of exposure remains high even after administration of currently accepted treatments[31]. Antibiotic therapy is frequently ineffective at curing anthrax patients, as re-emergence of and killing by the bacterium after its complete elimination from circulation has been observed[32].

We have investigated a nanotechnology-based approach to address these problems. We hypothesized that MP vehicles for delivering immune-modulating substances would sustainably promote leukocyte migration allowing the host to better clear an infectious agent. Current approaches for delivering CKs display poor results, in part due to the instability of CKs in dilute solutions and their rapid dissipation into the circulation. We show that our MPs represent a nontoxic vehicle with intrinsic immune-stimulatory activity capable of sustainably delivering CKs for directing immune responses.

We tested the prophylactic administration of CK-MPs as a proof-of-principle concept for their ability to overcome the immunosuppression induced by the bacterium. *In vivo* subcutaneous administration of the CK-MPs in a FP model of injection results in their accumulation both at the site of injection and to/within the local draining popliteal and inguinal LNs. At these sites, the functionally-protected CK becomes released from the MPs for a sustained period of more than 20 h. Direction of immune migration to these sites was beneficial, as *B. anthracis* spores injected in this model display the same pattern of distribution. We demonstrated that pre-treatment with CK-MPs conferred significant protection in spore-challenged animals. We have implicated both the MPs and their loaded CKs in promoting survival through similar/redundant mechanisms. The delivered CKs and the intrinsic ones induced by the MPs were critical for survival. Subsequent key factors contributing to the observed protection were the recruitment of neutrophils to the LN and FP, and the activation of tissue-resident Langerhans cells from the site of injection. We propose further investigation into possible clinical applications of CK-MPs as tools for achieving predictable, sustained modulation of immune activity.

REFERENCES

1. Kelly, M., Hwang, J. M. & Kubes, P. Modulating leukocyte recruitment in inflammation. *J. Allergy Clin. Immunol.* **120,** 3–10 (2007).
2. Sadik, C. D. & Luster, A. D. Lipid-cytokine-chemokine cascades orchestrate leukocyte recruitment in inflammation. *J. Leukoc. Biol.* **91,** 207–215 (2012).
3. Fernandez, E. J. & Lolis, and E. Structure, Function, and Inhibition of Chemokines. *Annu. Rev. Pharmacol. Toxicol.* **42,** 469–499 (2002).
4. Moser, B. & Loetscher, P. Lymphocyte traffic control by chemokines. *Nat. Immunol.* **2,** 123–128 (2001).
5. Mackay, C. R. Chemokines: immunology's high impact factors. *Nat. Immunol.* **2,** 95–101 (2001).
6. Skabytska, Y. & Biedermann, T. Cutaneous bacteria induce immunosuppression. *Oncotarget* **6,** 30441–30442 (2015).
7. Diaz, M. H. *et al.* Pseudomonas aeruginosa Induces Localized Immunosuppression during Pneumonia. *Infect. Immun.* **76,** 4414–4421 (2008).
8. Rabinovich, G. A., Gabrilovich, D. & Sotomayor, E. M. IMMUNOSUPPRESSIVE STRATEGIES THAT ARE MEDIATED BY TUMOR CELLS. *Annu. Rev. Immunol.* **25,** 267–296 (2007).
9. Houshmand, P. & Zlotnik, A. Therapeutic applications in the chemokine superfamily. *Curr. Opin. Chem. Biol.* **7,** 457–460 (2003).
10. Kohara, H. & Tabata, Y. JMBE-Review: Tissue Engineering Technology to Enhance Cell Recruitment for Regeneration Therapy. Available at: http://www.jmbe.org.tw/index.php?action=archives2&no=577. (Accessed: 6th June 2016)
11. Weert, M. van de, Hennink, W. E. & Jiskoot, W. Protein Instability in Poly(Lactic-co-Glycolic Acid) Microparticles. *Pharm. Res.* **17,** 1159–1167 (2000).
12. Zhu, G., Mallery, S. R. & Schwendeman, S. P. Stabilization of proteins encapsulated in injectable poly (lactide- co-glycolide). *Nat. Biotechnol.* **18,** 52–57 (2000).
13. Petros, R. A. & DeSimone, J. M. Strategies in the design of nanoparticles for therapeutic applications. *Nat. Rev. Drug Discov.* **9,** 615–627 (2010).
14. Tamburro, D. *et al.* Multifunctional Core–Shell Nanoparticles: Discovery of Previously Invisible Biomarkers. *J. Am. Chem. Soc.* **133,** 19178–19188 (2011).
15. Lemieux, P. *et al.* Block and graft copolymers and NanoGel copolymer networks for DNA delivery into cell. *J. Drug Target.* **8,** 91–105 (2000).

16. Hu, Y. *et al.* Cytosolic delivery mediated via electrostatic surface binding of protein, virus, or siRNA cargos to pH-responsive core-shell gel particles. *Biomacromolecules* **10,** 756–765 (2009).
17. Balmert, S. C. & Little, S. R. Biomimetic Delivery with Micro- and Nanoparticles. *Adv. Mater. Deerfield Beach Fla* **24,** 3757–3778 (2012).
18. Choudhury, R. P., Fuster, V. & Fayad, Z. A. Molecular, cellular and functional imaging of atherothrombosis. *Nat. Rev. Drug Discov.* **3,** 913–925 (2004).
19. Jones, C. D. & Lyon, L. A. Synthesis and Characterization of Multiresponsive Core−Shell Microgels. *Macromolecules* **33,** 8301–8306 (2000).
20. Luchini, A. *et al.* Smart Hydrogel Particles: Biomarker Harvesting: One-step affinity purification, size exclusion, and protection against degradation. *Nano Lett.* **8,** 350–361 (2008).
21. Kumar, S. & Punekar, N. S. High-throughput screening of dye-ligands for chromatography. *Methods Mol. Biol. Clifton NJ* **1129,** 53–65 (2014).
22. Denizli, A. & Pişkin, E. Dye-ligand affinity systems. *J. Biochem. Biophys. Methods* **49,** 391–416 (2001).
23. Sereikaite, J. & Bumelis, V.-A. Examination of dye-protein interaction by gel-permeation chromatography. *Biomed. Chromatogr. BMC* **20,** 195–199 (2006).
24. Longo, C. *et al.* Core-Shell Hydrogel Particles Harvest, Concentrate and Preserve Labile Low Abundance Biomarkers. *PLoS ONE* **4,** (2009).
25. Popova, T. G. *et al.* Chemokine-Releasing Nanoparticles for Manipulation of the Lymph Node Microenvironment. *Nanomaterials* **5,** 298–320 (2015).
26. Goncalves, D. M., de Liz, R. & Girard, D. Activation of Neutrophils by Nanoparticles. *ScientificWorldJournal* **11,** 1877–1885 (2011).
27. Guichard, A., Nizet, V. & Bier, E. New insights into the biological effects of anthrax toxins: linking cellular to organismal responses. *Microbes Infect. Inst. Pasteur* **14,** 97–118 (2012).
28. Abramova, F. A., Grinberg, L. M., Yampolskaya, O. V. & Walker, D. H. Pathology of inhalational anthrax in 42 cases from the Sverdlovsk outbreak of 1979. *Proc. Natl. Acad. Sci. U. S. A.* **90,** 2291–2294 (1993).
29. Grinberg, L. M., Abramova, F. A., Yampolskaya, O. V., Walker, D. H. & Smith, J. H. Quantitative Pathology of Inhalational Anthrax I: Quantitative Microscopic Findings. *Mod. Pathol.* **14,** 482–495 (2001).
30. Goldenberg, A., Shmueli, G., Caruana, R. A. & Fienberg, S. E. Early statistical detection of anthrax outbreaks by tracking over-the-counter medication sales. *Proc. Natl. Acad. Sci.* **99,** 5237–5240 (2002).
31. Spencer, R. C. Bacillus anthracis. *J. Clin. Pathol.* **56,** 182–187 (2003).
32. Barakat LA, Quentzel HL, Jernigan JA & et al. FAtal inhalational anthrax in a 94-year-old connecticut woman. *JAMA* **287,** 863–868 (2002).
33. Cleret-Buhot, A., Mathieu, J., Tournier, J.-N. & Quesnel-Hellmann, A. Both Lethal and Edema Toxins of Bacillus anthracis Disrupt the Human Dendritic Cell Chemokine Network. *PLoS ONE* **7,** (2012).
34. Paccani, S. R. *et al.* Anthrax toxins suppress T lymphocyte activation by disrupting antigen receptor signaling. *J. Exp. Med.* **201,** 325–331 (2005).

35. Tournier, J.-N. *et al.* Anthrax Edema Toxin Cooperates with Lethal Toxin to Impair Cytokine Secretion during Infection of Dendritic Cells. *J. Immunol.* **174,** 4934–4941 (2005).
36. During, R. L. *et al.* Anthrax Lethal Toxin Paralyzes Neutrophil Actin-Based Motility. *J. Infect. Dis.* **192,** 837–845 (2005).
37. Garraud, K. *et al.* Differential Role of the Interleukin-17 Axis and Neutrophils in Resolution of Inhalational Anthrax. *Infect. Immun.* **80,** 131–142 (2012).
38. Liu, S. *et al.* Anthrax toxin targeting of myeloid cells through the CMG2 receptor is essential for establishment of Bacillus anthracis infections in mice. *Cell Host Microbe* **8,** 455–462 (2010).
39. Hahn, B. L., Bischof, T. S. & Sohnle, P. G. Superficial exudates of neutrophils prevent invasion of Bacillus anthracis bacilli into abraded skin of resistant mice. *Int. J. Exp. Pathol.* **89,** 180–187 (2008).
40. Moayeri, M. *et al.* Inflammasome sensor Nlrp1b-dependent resistance to anthrax is mediated by caspase-1, IL-1 signaling and neutrophil recruitment. *PLoS Pathog.* **6,** e1001222 (2010).
41. Shannon, J. G., Ross, C. L., Koehler, T. M. & Rest, R. F. Characterization of Anthrolysin O, the Bacillus anthracis Cholesterol-Dependent Cytolysin. *Infect. Immun.* **71,** 3183–3189 (2003).
42. Wei, Z. *et al.* Characterization of Listeria monocytogenes Expressing Anthrolysin O and Phosphatidylinositol-Specific Phospholipase C from Bacillus anthracis. *Infect. Immun.* **73,** 6639–6646 (2005).
43. Popova, T. G., Millis, B., Chung, M.-C., Bailey, C. & Popov, S. G. Anthrolysin O and fermentation products mediate the toxicity of Bacillus anthracis to lung epithelial cells under microaerobic conditions. *Fems Immunol. Med. Microbiol.* **61,** 15–27 (2011).
44. Castro-Sesquen, Y. E. *et al.* Use of a Novel Chagas Urine Nanoparticle Test (Chunap) for Diagnosis of Congenital Chagas Disease. *PLoS Negl. Trop. Dis.* **8,** (2014).
45. Sundaram, P., Wower, J. & Byrne, M. E. A nanoscale drug delivery carrier using nucleic acid aptamers for extended release of therapeutic. *Nanomedicine Nanotechnol. Biol. Med.* **8,** 1143–1151 (2012).
46. Vulic, K., Pakulska, M. M., Sonthalia, R., Ramachandran, A. & Shoichet, M. S. Mathematical model accurately predicts protein release from an affinity-based delivery system. *J. Controlled Release* **197,** 69–77 (2015).
47. Hoare, T. R. & Kohane, D. S. Hydrogels in drug delivery: Progress and challenges. *Polymer* **49,** 1993–2007 (2008).
48. Mitragotri, S., Burke, P. A. & Langer, R. Overcoming the challenges in administering biopharmaceuticals: formulation and delivery strategies. *Nat. Rev. Drug Discov.* **13,** 655–672 (2014).
49. Danhier, F. *et al.* PLGA-based nanoparticles: An overview of biomedical applications. *J. Controlled Release* **161,** 505–522 (2012).

50. Setterstrom, J. A., Tice, T. R. & Myers, W. E. in *Recent Advances in Drug Delivery Systems* (eds. Anderson, J. M. & Kim, S. W.) 185–198 (Springer US, 1984). doi:10.1007/978-1-4613-2745-5_12
51. Dennis, M. S. *et al.* Albumin Binding as a General Strategy for Improving the Pharmacokinetics of Proteins. *J. Biol. Chem.* **277,** 35035–35043 (2002).
52. Subramanian, S. Dye-ligand affinity chromatography: the interaction of Cibacron Blue F3GA with proteins and enzymes. *CRC Crit. Rev. Biochem.* **16,** 169–205 (1984).
53. Böhme, U. & Scheler, U. Effective charge of bovine serum albumin determined by electrophoresis NMR. *Chem. Phys. Lett.* **435,** 342–345 (2007).
54. Graham, G. J. *et al.* Aggregation of the chemokine MIP-1 alpha is a dynamic and reversible phenomenon. Biochemical and biological analyses. *J. Biol. Chem.* **269,** 4974–4978 (1994).
55. Bancos, S. & Tyner, K. M. Evaluating the effect of assay preparation on the uptake of gold nanoparticles by RAW264.7 cells. *J. Nanobiotechnology* **12,** (2014).
56. Dunnick, K. M. *et al.* The effect of tungstate nanoparticles on reactive oxygen species and cytotoxicity in raw 264.7 mouse monocyte macrophage cells. *J. Toxicol. Environ. Health A* **77,** 1251–1268 (2014).
57. Sohaebuddin, S. K., Thevenot, P. T., Baker, D., Eaton, J. W. & Tang, L. Nanomaterial cytotoxicity is composition, size, and cell type dependent. *Part. Fibre Toxicol.* **7,** 22 (2010).
58. Harrell, M. I., Iritani, B. M. & Ruddell, A. Lymph Node Mapping in the Mouse. *J. Immunol. Methods* **332,** 170–174 (2008).
59. Randolph, G. J., Angeli, V. & Swartz, M. A. Dendritic-cell trafficking to lymph nodes through lymphatic vessels. *Nat. Rev. Immunol.* **5,** 617–628 (2005).
60. Willard-Mack, C. L. Normal Structure, Function, and Histology of Lymph Nodes. *Toxicol. Pathol.* **34,** 409–424 (2006).
61. Manolova, V. *et al.* Nanoparticles target distinct dendritic cell populations according to their size. *Eur. J. Immunol.* **38,** 1404–1413 (2008).
62. Yang, C.-W. & Unanue, E. R. Neutrophils control the magnitude and spread of the immune response in a thromboxane A2-mediated process. *J. Exp. Med.* **210,** 375–387 (2013).
63. Popova, T. G. *et al.* Whole Proteome Analysis of Mouse Lymph Nodes in Cutaneous Anthrax. *PLoS ONE* **9,** (2014).
64. Espinoza-González, N. A. *et al.* Efficacy of DA-7218, a New Oxazolidinone Prodrug, in the Treatment of Experimental Actinomycetoma Produced by Nocardia brasiliensis. *Molecules* **13,** 31–40 (2008).
65. Seil, J. T. & Webster, T. J. Antimicrobial applications of nanotechnology: methods and literature. *Int. J. Nanomedicine* **7,** 2767–2781 (2012).
66. Popova, T. G., Espina, V., Liotta, L. A. & Popov, S. G. Reverse-Phase Microarray Analysis Reveals Novel Targets in Lymph Nodes of Bacillus anthracis Spore-Challenged Mice. *PLoS ONE* **10,** (2015).
67. Natkunam, Y. The Biology of the Germinal Center. *ASH Educ. Program Book* **2007,** 210–215 (2007).

68. Musah, S., DeJarnett, N. & Hoyle, G. W. Tumor necrosis factor-α mediates interactions between macrophages and epithelial cells underlying proinflammatory gene expression induced by particulate matter. *Toxicology* **299,** 125–132 (2012).
69. Appelberg, R. T cell regulation of the chronic peritoneal neutrophilia during mycobacterial infections. *Clin. Exp. Immunol.* **89,** 120–125 (1992).
70. Gao, J. L. *et al.* Impaired host defense, hematopoiesis, granulomatous inflammation and type 1-type 2 cytokine balance in mice lacking CC chemokine receptor 1. *J. Exp. Med.* **185,** 1959–1968 (1997).
71. Ramos, C. D. L. *et al.* MIP-1alpha[CCL3] acting on the CCR1 receptor mediates neutrophil migration in immune inflammation via sequential release of TNF-alpha and LTB4. *J. Leukoc. Biol.* **78,** 167–177 (2005).
72. Huffnagle, G. B. *et al.* Leukocyte recruitment during pulmonary Cryptococcus neoformans infection. *Immunopharmacology* **48,** 231–236 (2000).
73. Huffnagle, G. B. *et al.* Afferent phase production of TNF-alpha is required for the development of protective T cell immunity to Cryptococcus neoformans. *J. Immunol.* **157,** 4529–4536 (1996).
74. Yan, W., Chen, W. & Huang, L. Mechanism of adjuvant activity of cationic liposome: Phosphorylation of a MAP kinase, ERK and induction of chemokines. *Mol. Immunol.* **44,** 3672–3681 (2007).
75. Das, S. T. *et al.* Monomeric and Dimeric CXCL8 Are Both Essential for In Vivo Neutrophil Recruitment. *PLoS ONE* **5,** (2010).
76. Ahuja, S. K., Lee, J. C. & Murphy, P. M. CXC chemokines bind to unique sets of selectivity determinants that can function independently and are broadly distributed on multiple domains of human interleukin-8 receptor B. Determinants of high affinity binding and receptor activation are distinct. *J. Biol. Chem.* **271,** 225–232 (1996).
77. Holmes, W. E., Lee, J., Kuang, W. J., Rice, G. C. & Wood, W. I. Structure and functional expression of a human interleukin-8 receptor. *Science* **253,** 1278–1280 (1991).
78. Murphy, P. M. & Tiffany, H. L. Cloning of complementary DNA encoding a functional human interleukin-8 receptor. Science. 1991. 253: 1280-1283. *J. Immunol. Baltim. Md 1950* **183,** 2898–2901 (2009).
79. Ren, M. *et al.* Polymerization of MIP-1 chemokine (CCL3 and CCL4) and clearance of MIP-1 by insulin-degrading enzyme. *EMBO J.* **29,** 3952–3966 (2010).
80. O'Grady, N. P. *et al.* Detection of Macrophage Inflammatory Protein (MIP)-1α and MIP-β during Experimental Endotoxemia and Human Sepsis. *J. Infect. Dis.* **179,** 136–141 (1999).
81. Massena, S. *et al.* A chemotactic gradient sequestered on endothelial heparan sulfate induces directional intraluminal crawling of neutrophils. *Blood* **116,** 1924–1931 (2010).
82. Nauseef, W. M. & Borregaard, N. Neutrophils at work. *Nat. Immunol.* **15,** 602–611 (2014).
83. Nathan, C. Neutrophils and immunity: challenges and opportunities. *Nat. Rev. Immunol.* **6,** 173–182 (2006).

84. Brinkmann, V. *et al.* Neutrophil extracellular traps kill bacteria. *Science* **303,** 1532–1535 (2004).
85. Welkos, S. L., Trotter, R. W., Becker, D. M. & Nelson, G. O. Resistance to the Sterne strain of B. anthracis: phagocytic cell responses of resistant and susceptible mice. *Microb. Pathog.* **7,** 15–35 (1989).
86. Mayer-Scholl, A. *et al.* Human Neutrophils Kill Bacillus anthracis. *PLOS Pathog* **1,** e23 (2005).
87. Lisanby, M. W. *et al.* Cathelicidin Administration Protects Mice from Bacillus anthracis Spore Challenge. *J. Immunol. Baltim. Md 1950* **181,** 4989–5000 (2008).
88. Popova, T. G. *et al.* Reverse-Phase Phosphoproteome Analysis of Signaling Pathways Induced by Rift Valley Fever Virus in Human Small Airway Epithelial Cells. *PLOS ONE* **5,** e13805 (2010).
89. Yang, Q., Ghose, P. & Ismail, N. Neutrophils Mediate Immunopathology and Negatively Regulate Protective Immune Responses during Fatal Bacterial Infection-Induced Toxic Shock. *Infect. Immun.* **81,** 1751–1763 (2013).
90. Zeilhofer, H. U. & Schorr, W. Role of interleukin-8 in neutrophil signaling. *Curr. Opin. Hematol.* **7,** 178–182 (2000).
91. Palomäki, J., Karisola, P., Pylkkänen, L., Savolainen, K. & Alenius, H. Engineered nanomaterials cause cytotoxicity and activation on mouse antigen presenting cells. *Toxicology* **267,** 125–131 (2010).
92. Santos, D. M. *et al.* PLGA nanoparticles loaded with KMP-11 stimulate innate immunity and induce the killing of Leishmania. *Nanomedicine Nanotechnol. Biol. Med.* **9,** 985–995 (2013).
93. Meraz, I. M. *et al.* Activation of the Inflammasome and Enhanced Migration of Microparticle-Stimulated Dendritic Cells to the Draining Lymph Node. *Mol. Pharm.* **9,** 2049–2062 (2012).
94. Li, Y. & Boraschi, D. Endotoxin contamination: a key element in the interpretation of nanosafety studies. *Nanomed.* **11,** 269–287 (2016).
95. Mejia, J. S., Toot-Zimmer, A. L., Schultheiss, P. C., Beaty, B. J. & Titus, R. G. BluePort: A Platform to Study the Eosinophilic Response of Mice to the Bite of a Vector of Leishmania Parasites, Lutzomyia longipalpis Sand Flies. *PLOS ONE* **5,** e13546 (2010).
96. Youmans, A. S. & Youmans, G. P. Effect of polybasic amines on the immunogenicity of mycobacterial ribonucleic acid. *Infect. Immun.* **6,** 798–804 (1972).
97. Townson, J. L. *et al.* Re-Examining the Size/Charge Paradigm: Differing In Vivo Characteristics of Size and Charge-Matched Mesoporous Silica Nanoparticles. *J. Am. Chem. Soc.* **135,** 16030–16033 (2013).
98. Broos, S. *et al.* Immunomodulatory nanoparticles as adjuvants and allergen-delivery system to human dendritic cells: Implications for specific immunotherapy. *Vaccine* **28,** 5075–5085 (2010).
99. Xiang, S. D. *et al.* Nanoparticles modify dendritic cell homeostasis and induce non-specific effects on immunity to malaria. *Trans. R. Soc. Trop. Med. Hyg.* **109,** 70–76 (2015).

100. Ramos, C. D. L. *et al.* Neutrophil recruitment in immunized mice depends on MIP-2 inducing the sequential release of MIP-1alpha, TNF-alpha and LTB(4). *Eur. J. Immunol.* **36,** 2025–2034 (2006).
101. Reichel, C. A. *et al.* Ccl2 and Ccl3 mediate neutrophil recruitment via induction of protein synthesis and generation of lipid mediators. *Arterioscler. Thromb. Vasc. Biol.* **29,** 1787–1793 (2009).
102. Simon, H.-U. Neutrophil apoptosis pathways and their modifications in inflammation. *Immunol. Rev.* **193,** 101–110 (2003).
103. Charmoy, M. *et al.* Neutrophil-Derived CCL3 Is Essential for the Rapid Recruitment of Dendritic Cells to the Site of Leishmania major Inoculation in Resistant Mice. *PLOS Pathog.* **6,** e1000755 (2010).
104. Gouwy, M. *et al.* Serum amyloid A chemoattracts immature dendritic cells and indirectly provokes monocyte chemotaxis by induction of cooperating CC and CXC chemokines. *Eur. J. Immunol.* **45,** 101–112 (2015).
105. Ascough, S., Ingram, R. J. & Altmann, D. M. Anthrax Lethal Toxin and the Induction of CD4 T Cell Immunity. *Toxins* **4,** 878–899 (2012).
106. Kouris, A. *et al.* Proinflammatory cytokine responses in patients with psoriasis. *Eur. Cytokine Netw.* **25,** 63–68 (2014).
107. Katschke, K. J. *et al.* Differential expression of chemokine receptors on peripheral blood, synovial fluid, and synovial tissue monocytes/macrophages in rheumatoid arthritis. *Arthritis Rheum.* **44,** 1022–1032 (2001).
108. Zimmermann, H. W. *et al.* Functional Contribution of Elevated Circulating and Hepatic Non-Classical CD14+CD16+ Monocytes to Inflammation and Human Liver Fibrosis. *PLoS ONE* **5,** (2010).
109. Dimachkie, M. M., Barohn, R. J. & Amato, A. Idiopathic Inflammatory Myopathies. *Neurol. Clin.* **32,** 595–628 (2014).
110. Glass, C. K., Saijo, K., Winner, B., Marchetto, M. C. & Gage, F. H. Mechanisms Underlying Inflammation in Neurodegeneration. *Cell* **140,** 918–934 (2010).
111. Akiyama, H. Inflammatory response in Alzheimer's disease. *Tohoku J. Exp. Med.* **174,** 295–303 (1994).
112. Tisoncik, J. R. *et al.* Into the Eye of the Cytokine Storm. *Microbiol. Mol. Biol. Rev. MMBR* **76,** 16–32 (2012).
113. Gratton, S. E. A. *et al.* The effect of particle design on cellular internalization pathways. *Proc. Natl. Acad. Sci. U. S. A.* **105,** 11613–11618 (2008).
114. Gregory, A. E., Titball, R. & Williamson, D. Vaccine delivery using nanoparticles. *Front. Cell. Infect. Microbiol.* **3,** (2013).
115. Weissleder, R., Nahrendorf, M. & Pittet, M. J. Imaging macrophages with nanoparticles. *Nat. Mater.* **13,** 125–138 (2014).
116. Getts, D. R., Shea, L. D., Miller, S. D. & King, N. J. C. Harnessing nanoparticles for immune modulation. *Trends Immunol.* **36,** 419–427 (2015).
117. Chiu, H.-W. *et al.* Cationic polystyrene nanospheres induce autophagic cell death through the induction of endoplasmic reticulum stress. *Nanoscale* **7,** 736–746 (2015).

118. Hwang, T.-L., Aljuffali, I. A., Lin, C.-F., Chang, Y.-T. & Fang, J.-Y. Cationic additives in nanosystems activate cytotoxicity and inflammatory response of human neutrophils: lipid nanoparticles versus polymeric nanoparticles. *Int. J. Nanomedicine* **10,** 371–385 (2015).
119. Xia, T., Kovochich, M., Liong, M., Zink, J. I. & Nel, A. E. Cationic polystyrene nanosphere toxicity depends on cell-specific endocytic and mitochondrial injury pathways. *ACS Nano* **2,** 85–96 (2008).
120. Getts, D. R. *et al.* Microparticles bearing encephalitogenic peptides induce T-cell tolerance and ameliorate experimental autoimmune encephalomyelitis. *Nat. Biotechnol.* **30,** 1217–1224 (2012).
121. Getts, D. R. *et al.* Therapeutic Inflammatory Monocyte Modulation Using Immune-Modifying Microparticles. *Sci. Transl. Med.* **6,** 219ra7 (2014).
122. Hunter, Z. *et al.* A Biodegradable Nanoparticle Platform for the Induction of Antigen-Specific Immune Tolerance for Treatment of Autoimmune Disease. *ACS Nano* **8,** 2148–2160 (2014).

BIOGRAPHY

Allison Teunis graduated from Gar-Field Senior High School, Woodbridge, Virginia in 2007. She received her Bachelor of Science in Biology from James Madison University, Harrisonburg, Virginia in 2011. She interned at the Virginia Department of Agriculture and Consumer Services during her senior year of college, where she was inspired to change pursue a career in microbiology.